UCLA
COMPUTATIONAL AND APPLIED MATHEMATICS

Singular Perturbation Analysis of Boundary-Value Problems for Differential-Difference Equations V. Small Shifts with Layer Behavior

Charles G. Lange
Robert M. Miura

March 1992

CAM Report 92-12

Department of Mathematics
University of California, Los Angeles
Los Angeles, CA. 90024-1555

SINGULAR PERTURBATION ANALYSIS OF BOUNDARY-VALUE PROBLEMS FOR DIFFERENTIAL-DIFFERENCE EQUATIONS V. SMALL SHIFTS WITH LAYER BEHAVIOR*

Dedicated to the Memory of our Friend, Hubertus J. Weinitschke

CHARLES G. LANGE† and ROBERT M. MIURA‡

Abstract. In this paper we initiate an investigation of boundary-value problems for singularly perturbed linear second-order differential-difference equations with small shifts, i.e., where the second-order derivative is multiplied by a small parameter and the shift depends on the small parameter. Similar boundary-value problems are associated with expected first-exit times of the membrane potential in models for neurons. In particular we focus on problems with solutions which exhibit layer behavior at one or both of the boundaries. The analyses of the layer equations using Laplace transforms lead to novel results. It is shown that the order of magnitude of the shift must be at least as large as that of the layer thickness in order for the shift to affect the solution to leading order. [In the companion paper, "Singular perturbation analysis of boundary-value problems for differential-difference equations VI. Small shifts with rapid oscillations", this journal, this issue, pp. , we study similar boundary-value problems with solutions which exhibit rapid oscillations.]

Key words. differential-difference equations, singular perturbations, boundary-value problems, small shifts, layer behavior, Laplace transforms, exponential polynomials, first-exit times, action potentials

AMS(MOS) subject classifications. 34K10, 34K25, 44A10, 30C15, 92C20

* This work was supported in part by (CGL) the National Science Foundation under grant DMS 88-15467, the Office of Naval Research under grant N000 14-86-K-0691 and by (RMM) the Natural Sciences and Engineering Research Council of Canada under Grant 5-84559.

† Department of Mathematics, University of California, Los Angeles, California 90024.

‡ Department of Mathematics and Institute of Applied Mathematics, University of British Columbia, Vancouver, British Columbia, Canada V6T 1Z2.

1. Introduction. Generation of action potentials in nerve cells by random synaptic inputs in the dendrites can be modelled as a first-exit time problem. The case of inputs distributed as a Poisson process with exponential decay between the inputs was formulated by Stein [16] and studied by Tuckwell [17], [18] and by Wilbur and Rinzel [20]. If, in addition, there are inputs which can be modelled as a Wiener process with variance parameter σ and drift parameter μ, then the problem for the expected first-exit time, y, given the initial membrane potential, $x \in (x_1, x_2)$, can be formulated as a general boundary-value problem (BVP) for the linear second-order differential-difference equation (DDE)

$$\frac{\sigma^2}{2}y''(x) + (\mu - x)y'(x) + \lambda_E y(x + a_E) + \lambda_I y(x - a_I) - (\lambda_E + \lambda_I)y(x) = -1, \tag{1.1}$$

where the values $x = x_1$ and $x = x_2$ correspond to the inhibitory reversal potential and to the threshold value of membrane potential for action potential generation. The first-derivative term $-xy'$ corresponds to exponential decay between synaptic inputs. The undifferentiated terms correspond to excitatory and inhibitory synaptic inputs modelled as Poisson processes with mean rates λ_E and λ_I, respectively, and produce jumps in the membrane potential of amounts a_E and $-a_I$, respectively, which are small quantities and could depend on voltage. The boundary condition is

$$y(x) \equiv 0, \quad x \notin (x_1, x_2). \tag{1.2}$$

In this paper we initiate an investigation of BVPs for DDEs with small shifts. Our long range goal is to analyze problems associated with the BVP (1.1)-(1.2) for expected first-exit times of the membrane potential in models of neurons. Our previous studies of boundary-value problems for singularly perturbed differential-difference equations have

always considered shifts of fixed length (negative or both negative and positive) ([7]-[10], [12]). Solutions of such BVPs for DDEs exhibit a variety of interesting phenomena including boundary and interior layers, rapid oscillations, resonance, turning point behavior, and nonuniqueness and/or nonexistence for nonlinear DDEs. We are carrying out these studies of BVPs for singularly perturbed DDEs to encourage the use of DDE models in the physical and biological sciences.

One method for solving BVPs for second-order linear DDEs is to use the method of steps, i.e., sequentially solve problems on successive intervals explicitly and evaluate constants of integration by matching boundary conditions and imposing continuity of the solution and its derivative at interior points. However, with small shifts on a unit interval, the method of steps is impractical for DDEs involving only negative (or only positive) shift terms, and impossible for DDEs of mixed type, i.e., with both negative and positive shift terms. As pointed out by O'Malley [14] and as we demonstrate here, the naive approach of simply expanding the shift terms in Taylor series and truncating can lead to misleading results. Even the numerical solution of these BVPs is no longer straightforward. Instead perturbation methods are more appropriate and some of these have been given by Vasil'eva [19], Cooke and Meyer [4], and O'Malley [13].

Specifically, here we analyze modified versions of classical singularly perturbed ODEs [3], [5], [15]. In particular, the method of matched asymptotic expansions [6], developed for ODEs, is extended to the study on $0 < x < 1$ of BVPs for linear DDEs with small shifts which have solutions that exhibit layer behavior. The studies here using singular perturbation methods coupled with numerical computations are not meant to be exhaustive

and the most general cases are not examined. Rather we focus on two representative model problems to illustrate the ideas and make them as transparent as possible. Solutions of these model problems contain the features of solutions of more general equations.

There are novel results in analyzing BVPs for singularly perturbed ODEs with small shifts with solutions exhibiting layer behavior. The most important findings are: 1) even if the shifts are small, their effects may contribute to the leading-order approximate solutions; 2) the layer behavior can change its character and even be destroyed as the shifts increase but remain small; and 3) for some problems, the Laplace transform method used to analyze the boundary-layer solutions is applicable even when there are poles in the right-half s-plane going off to infinity.

For layer problems, the shift affects the layer solution to leading order only if the magnitude of the shift is at least as large as the layer thickness which is small. Thus small shifts also could play an important role for partial differential equations with layer solutions. In contrast, for rapidly oscillating problems (cf. the companion paper [11]), the shift affects the solution to leading order even when the shift is small compared to the scale of the oscillations.

Statements of the BVPs for DDEs to be investigated in this paper are given in Section 2. Problems with solutions exhibiting layer behavior at the left end or the right end and at both ends are analyzed in Sections 3 and 4, respectively, using a combination of singular perturbation methods, Laplace transforms, and numerical computations. When the shifts are $O(\epsilon)$ with coefficients of $O(1)$ the layer structures of the solutions discussed here are no longer preserved. Oscillations previously confined to the layer regions can extend into

the outer region and the solution method presented here fails to give the correct inner and outer solutions. These solutions for the DDE problems as well as others exhibiting rapid oscillations are treated in the companion paper [11] using a WKB method.

2. Statements of the problems. In this section, we state the BVPs for the two classes of singularly perturbed DDEs to be studied in this paper. When the shift is zero, the solutions of the BVPs for the corresponding ODEs exhibit layer behavior. Here we will examine questions on the effects of small shifts on this behavior as well as construct leading-order approximate solutions. In particular, when can the shifts be ignored to leading order and when do they modify the qualitative behavior of the layers? In the outer regions we find that it is appropriate to expand the shifted terms. However, the shifts affect the layer solutions when the shifts are of the same order of magnitude (in ε) as the layer width and we cannot expand the shifted term.

Specifically BVPs for two general classes of DDEs are investigated. The BVP for the first class of DDEs is

$$\varepsilon y''(x;\varepsilon) + a(x)y'(x-\delta(\varepsilon);\varepsilon) + b(x)y(x;\varepsilon) = f(x), \tag{2.1}$$

on $0 < x < 1$, $0 < \varepsilon \ll 1$, and $0 \leq \delta(\varepsilon) \ll 1$, subject to the interval and boundary conditions

$$y(x;\varepsilon) = \phi(x) \quad \text{on} \quad -\delta(\varepsilon) \leq x \leq 0, \quad y(1;\varepsilon) = \gamma, \tag{2.2}$$

respectively, where $a(x)$, $b(x)$, $f(x)$, $\delta(\varepsilon)$, and $\phi(x)$ are smooth functions and γ is a constant. This will be referred to as Model Problem 1. For a function $y(x;\varepsilon)$ to constitute a "smooth" solution of Model Problem 1, it must satisfy (2.1)-(2.2), be continuous on [0,1], and be continuously differentiable on (0,1).

This class of DDEs, (2.1), contains a negative shift only in the first-order derivative term. For $\delta(\varepsilon) \equiv 0$, the corresponding ODE has solutions with a layer on the left or on the right for $a(x) > 0$ or $a(x) < 0$ on $0 \leq x \leq 1$, respectively. The layer is maintained for $\delta(\varepsilon)$ not zero but sufficiently small. These problems, $a(x) > 0$ or $a(x) < 0$, are analyzed in Sections 3.1 and 3.2, respectively. If $a(x)$ changes sign in $0 < x < 1$, then the solution can exhibit more complicated turning point behavior. Such problems are not analyzed in this paper.

The second class of DDEs is given by

$$\varepsilon^2 y''(x;\varepsilon) + \alpha(x)y(x-\delta(\varepsilon);\varepsilon) + \omega(x)y(x;\varepsilon) + \beta(x)y(x+\eta(\varepsilon);\varepsilon) = f(x), \tag{2.3}$$

(note the coefficient of y'' is ε^2 and not ε as in (2.1)) on $0 < x < 1, 0 < \varepsilon \ll 1, 0 \leq \delta(\varepsilon) \ll 1$, and $0 \leq \eta(\varepsilon) << 1$, subject to the interval conditions

$$\begin{aligned} y(x;\varepsilon) &= \phi(x) \quad \text{on} \quad -\delta(\varepsilon) \leq x \leq 0, \\ y(x;\varepsilon) &= \psi(x) \quad \text{on} \quad 1 \leq x \leq 1+\eta(\varepsilon), \end{aligned} \tag{2.4}$$

where $\alpha(x)$, $\omega(x)$, $\beta(x)$, $f(x)$, $\delta(\varepsilon)$, $\eta(\varepsilon)$, $\phi(x)$, and $\psi(x)$ are smooth functions. This problem will be referred to as Model Problem 2. A function $y(x;\varepsilon)$ is a smooth solution of Model Problem 2, if it satisfies (2.3)-(2.4), is continuous on [0,1], and is continuously differentiable on (0,1). For convenience, it is assumed that $\phi(x) \equiv 1$ and $\psi(x) \equiv$ constant. Also, since $f(x)$ contributes only a constant forcing term in the layer regions, it is convenient to assume that $f(x) \equiv 1$ in the example problems.

In Section 4, BVPs of the DDEs, (2.3), of mixed type (i.e., containing a term with a negative shift and a term with a positive shift) with solutions having boundary layers at both ends of the interval are studied, i.e., with $\alpha(x) + \omega(x) + \beta(x) < 0$ on $0 < x < 1$.

If the shifts, $\delta(\varepsilon)$ and $\eta(\varepsilon)$, are both zero, and $\alpha(x) + \omega(x) + \beta(x) < 0$ on $0 < x < 1$, then the solution of the corresponding ODE has layers at both the left and right ends. Since DDEs of mixed type are difficult to solve, first the problem with $\beta(x) \equiv 0$ is treated separately and incorporates much of the information already derived in Sections 3.1 and 3.2. Then DDEs of mixed type, i.e., with $\beta(x) \not\equiv 0$, with layers at both sides are examined. The novelty of this class of equations is that the negative and positive shifts need not be the same. The investigations here examine the solutions when the shifts are not zero and determine when the shifts can be ignored to leading order and what are their sizes when they begin to influence the qualitative features of the solutions. [If $\alpha(x)+\omega(x)+\beta(x) > 0$ on $0 < x < 1$, then the solution of the corresponding ODE has oscillatory solutions all across the interval, cf. the companion paper [11].].

To determine when the shift becomes important to leading order, expand the shifted terms in (2.1) and (2.3) in Taylor series for small shifts. In (2.1), to leading order, the effects of the shift may be ignored if $\delta(\varepsilon) = o(\varepsilon)$. Thus it will be assumed that $\delta(\varepsilon) \equiv \tau\varepsilon$ with $\tau = O(1)$. On the other hand, in (2.3), to leading order, the effects of the shift only may be ignored if $\delta(\varepsilon)$ and $\eta(\varepsilon)$ are both $o(\varepsilon)$. For the analysis here it is assumed that $\delta(\varepsilon) \equiv \tau\varepsilon$ and $\eta(\varepsilon) \equiv \mu\varepsilon$ with τ and μ both of $O(1)$.

The results presented here can be extended in a variety of directions. Problems with several shifts can be treated with the Laplace transform method used here. The added complexity would be translated into the investigation of more complicated exponential polynomials, cf. Bellman and Cooke [2]. Addition of terms such as $y(x - \delta(\varepsilon); \varepsilon)$ in (2.1) and first-order derivative terms to (2.3) could be handled using similar techniques. The

essential features of the methods are illustrated in the examples chosen below. Other extensions, e.g., nonlinearity, are more difficult to treat.

Since the singular perturbation techniques developed here are formal, it is essential to test their validity using other results. In lieu of exact solutions which are unobtainable in general, accurate numerically computed solutions are compared to the asymptotic results. Previously [7]-[10], BVPs for DDEs with a shift of one were solved numerically using COLSYS [1] on intervals of length 1.5 or 2 by collapsing the interval into a shorter subinterval, see [1] and [7] for details. In the problems treated here with small shifts on a unit interval, it is impractical if not impossible to collapse the interval into a smaller subinterval and a new method for obtaining numerical solutions is required. The numerical treatment of the problems studied here is sketched in Appendix 1.

3. Layer behavior for Model Problem 1. In this section, different versions of Model Problem 1 are studied for which the solutions to the BVPs of the corresponding ODEs, i.e., with zero shifts, exhibit layer behavior. In particular, the analysis includes determination of leading-order outer solutions and Laplace transform analyses of the layer solutions. In Sections 3.1 and 3.2, the DDE (2.1) is examined where it is convenient to set $f(x)$ equal to zero (it can be included without any difficulty to leading order). This class of DDEs has the shift in a first-order derivative term where the shift has its most significant effects. If the shift, $\delta(\varepsilon)$, is zero, then there is a layer at $x = 0$ or at $x = 1$ for $a(x) > 0$ or $a(x) < 0$ on $0 < x < 1$, respectively. The study here focuses on the effects of $\delta(\varepsilon)$ on this layer behavior. Adding a term $y(x - \delta(\varepsilon); \varepsilon)$ would not alter the leading-order solution in the layer or outer regions. To illustrate the general technique, in Section 3.1

the problem with $a(x) > 0$ having solutions with a boundary layer only at $x = 0$ will be solved to leading order. The same general class of DDEs except with $a(x) < 0$ is treated in Section 3.2. Use of the Laplace transform in this case introduces several novel difficulties.

3.1. Layer on the left. Consider the class of DDEs given by (2.1) ($f(x) \equiv 0$) with $a(x) > 0$ on $0 \leq x \leq 1$. Since the crucial order of $\delta(\varepsilon)$ is $O(\varepsilon)$ for its effect to appear at leading order, we set $\delta(\varepsilon) = \tau\varepsilon$ with $\tau = O(1)$. Provided τ is not too large, the layer structure is modified but maintained, so there is a boundary layer at $x = 0$. For convenience, it is assumed that $\phi(x) \equiv 1$. Also it is convenient to assume $f(x) \equiv 0$ since its effect is of higher order in the layer solutions. Numerical solutions for the case $a(x) = 1$, $b(x) = 1$, $f(x) = 0$, $\phi(x) = 1$, $\gamma = 1$, and $\varepsilon = 0.01$ with $\tau = 0, 0.7, 1.5$, and 2.5 are shown in Figures 1a, b, c, and d, respectively. Note that for $\tau = 0.7$, the solution shown in Figure 1b is still of layer type but oscillations have developed within the layer. For $\tau = 1.5$, the oscillations shown in Figure 1c spread into the outer solution region and the layer structure is destroyed. For $\tau = 2.5$, the oscillations shown in Figure 1d grow exponentially across the interval reaching an amplitude of approximately 14,700 near $x = 1$. A WKB method is developed in [11] to solve these cases.

If $\delta(\varepsilon) \equiv 0$, then the BVP for (2.1) - (2.2), reduces to an ODE problem with a boundary layer at $x = 0$. The outer solution in this case is given by

$$y(x;\varepsilon) = \gamma \exp\left[\int_x^1 \frac{b(t)}{a(t)}\, dt\right] + O(\varepsilon) \quad \text{as} \quad \varepsilon \to 0, \tag{3.1}$$

uniformly in x on $0 < x_0 \leq x \leq 1$ for some $x_0 > 0$. A standard singular perturbation analysis of the boundary layer problem in the new variables

$$\tilde{x} \equiv \frac{x}{\varepsilon}, \quad \tilde{y}(\tilde{x};\varepsilon) \equiv y(\varepsilon\tilde{x};\varepsilon) \tag{3.2}$$

yields the solution

$$\tilde{y}(\tilde{x};\varepsilon) = \Gamma + \{\phi(0) - \Gamma\}e^{-a(0)\tilde{x}} + O(\varepsilon) \tag{3.3}$$

on $0 < \tilde{x} < \infty$ as $\varepsilon \to 0$, where

$$\Gamma \equiv \gamma \exp\left[\int_0^1 \frac{b(t)}{a(t)}\, dt\right]. \tag{3.4}$$

This solution satisfies the left boundary condition and matches the outer solution as $\tilde{x} \to \infty$ and $x \to 0$.

For $\delta(\varepsilon) = \tau\varepsilon > 0$, with τ not too large, the method using layer regions for solving the BVP is demonstrated and is used on most of the layer problems analyzed here. In the outer region, $0 < x \leq 1$, expand the shifted term as

$$y'(x - \delta(\varepsilon);\varepsilon) = y'(x;\varepsilon) - \delta(\varepsilon)y''(x;\varepsilon) + \ldots \quad \text{as} \quad \varepsilon \to 0, \tag{3.5}$$

and assume the solution has the form

$$y(x;\varepsilon) \sim \sum_{j=0}^{\infty} y_j(x)\varepsilon^j \quad \text{as} \quad \varepsilon \to 0. \tag{3.6}$$

Thus the sequence of problems satisfied by y_j is

$$Ly_0 \equiv a(x)y_0'(x) + b(x)y_0(x) = 0, \quad y_0(1) = \gamma, \tag{3.7}$$

$$Ly_j = a(x)\sum_{k=1}^{j}(-1)^{k+1}\frac{\tau^k}{k!}y_{j-k}^{(k+1)}(x) - y_{j-1}''(x), \quad y_j(1) = 0, \quad j = 1, 2, \ldots . \tag{3.8}$$

The leading-order equation (3.7) is identical to that for the outer equation when $\delta(\varepsilon) \equiv 0$, and hence has the solution given by (3.1). The effects of the delay are contained in the higher-order terms.

For the boundary layer at $x = 0$, introduce a scaled independent variable and new dependent variable by

$$\tilde{x} \equiv \frac{x}{\varepsilon}, \quad \tilde{y}(\tilde{x};\varepsilon) \equiv y(\varepsilon\tilde{x};\varepsilon), \tag{3.9}$$

so that (2.1) becomes

$$\tilde{y}''(\tilde{x};\varepsilon) + a(\varepsilon\tilde{x})\tilde{y}'(\tilde{x}-\tau;\varepsilon) + \varepsilon b(\varepsilon\tilde{x})\tilde{y}(\tilde{x};\varepsilon) = 0 \tag{3.10}$$

on $0 < \tilde{x} < \infty$. We assume that

$$\tilde{y}(\tilde{x};\varepsilon) \sim \sum_{j=0}^{\infty} \tilde{y}_j(\tilde{x})\varepsilon^j \quad \text{as} \quad \varepsilon \to 0 \tag{3.11}$$

Without loss of generality in the layer solution, we assume $a(0) = 1$, then the leading-order equation for $\tilde{y}_0$ is given by

$$\tilde{y}_0''(\tilde{x}) + \tilde{y}_0'(\tilde{x}-\tau) = 0, \quad \tilde{y}_0(0) = 1, \tag{3.12}$$

and matching with the outer solution requires

$$\lim_{\tilde{x}\to\infty} \tilde{y}_0(\tilde{x}) = \Gamma. \tag{3.13}$$

Integrating (3.12) once and applying both the boundary condition at $\tilde{x} = 0$ and the matching conditions (3.13) yields

$$\begin{aligned} \tilde{y}_0'(\tilde{x}) + \tilde{y}_0(\tilde{x}-\tau) &= \tilde{y}_0'(0) + 1 \\ &= \Gamma \end{aligned} \tag{3.14}$$

This permits determination of the unknown slope, $\tilde{y}_0'(0)$,

$$\tilde{y}_0'(0) = \Gamma - 1. \tag{3.15}$$

To solve (3.14), use the Laplace transform $\tilde{Y}_0(s) = \mathcal{L}[\tilde{y}_0(\tilde{x})]$, with solution

$$\tilde{Y}_0(s) = \frac{1}{s} + \frac{\Gamma - 1}{s(s + e^{-\tau s})}. \tag{3.16}$$

Thus the leading-order solution, $\tilde{y}_0$, is obtained by a straightforward inversion of (3.16) as an infinite sum of residues. These residues are evaluated at $s = 0$ and at the infinite number of roots of the exponential polynomial, cf. Bellman and Cooke [2],

$$P(s;\tau) \equiv s + e^{-\tau s} = 0. \tag{3.17}$$

Detailed information and asymptotic results for the roots, s_n, of (3.17) are given in Appendix 2.1. In particular, for each value of τ in $0 < \tau < 1/e$, there are two distinct negative real roots, say s_0 and s_1, located at $-\infty < s_0 < -e$ and $-e < s_1 < -1$, see Figure 2a. For $\tau = 0, s_0 = -\infty$ and $s_1 = -1$. All other roots occur in complex conjugate pairs with $\epsilon + \text{Re } s_n << 1$, $n = 2, 3, \ldots$. For $\tau = 1/e$, the two negative real roots coelesce at $s_1 = -e$ and as τ is increased the roots split into a complex conjugate pair, say s_1 and $\bar{s}_1$, still with $\epsilon + \text{Re } s_n << 1$, $n = 2, 3, \ldots$, see Figure 2b. At $\tau = \pi/2$, Re $s_1 = 0$ with s_1 and $\bar{s}_1$ crossing into the right half plane for $\tau > \pi/2$.

The inversion of $\tilde{Y}_0(s)$ from (3.16) thus yields $\tilde{y}_0$ in the form

$$\tilde{y}_0(\tilde{x}) = \Gamma + c_0 e^{s_0 \tilde{x}} + c_1 e^{s_1 \tilde{x}} + \sum_{n=2}^{\infty} \left(c_n e^{s_n \tilde{x}} + \bar{c}_n e^{\bar{s}_n \tilde{x}} \right), \tag{3.18}$$

where bars indicate complex conjugates, and the c_n are given by (using (3.17))

$$c_n = \frac{\Gamma - 1}{s_n(1 + \tau s_n)}, \quad n = 0, 1, 2, \ldots . \tag{3.19}$$

The terms with coefficients c_0 and c_1 are displayed separately because, as noted above, for $0 < \tau < 1/e$, the roots s_0 and s_1 are real and distinct.

Thus when $0 < \tau < 1/e$, a numerically accurate approximation of the boundary layer solution for large $\tilde{x}$ is given by

$$\tilde{y}(\tilde{x};\varepsilon) \sim \tilde{y}_0(\tilde{x}) \sim \Gamma + c_0 e^{s_0 \tilde{x}} + c_1 e^{s_1 \tilde{x}}, \quad \tilde{x} \to \infty, \quad \varepsilon \to 0. \tag{3.20}$$

For $0 < \tau \ll 1$, the second term in (3.20) is exponentially small and $\tilde{y}$ agrees to leading order with (3.3). This agreement forms the basis of our observation that the order of the shift must be of the same size as the layer for the shift to affect the solution to leading order. If $\tau > 1/e$, then s_0 and s_1 are complex conjugates and c_0 and s_0 are replaced by $\overline{c}_1$ and $\overline{s}_1$, respectively. Note that the leading-order layer solution does not depend on either b or f except through the constant Γ.

The accuracy of the approximations in the layer and outer regions are checked by evaluating the slope $\tilde{y}'(0)$ for the examples corresponding to Figures 1a and b, namely $\tilde{y}'(0)$ has the numerical values 1.7008 and 1.7124 for $\tau = 0$ and 0.7, respectively. The approximation (3.15) yields the value $\tilde{y}'(0) \simeq 1.7183$.

[When τ is close to $\pi/2$ with Re $s_1 = O(\varepsilon)$ or positive, the amplitude of the oscillation which occurs in (3.18) does not decay sufficiently rapidly to allow matching with the assumed outer solution (3.1) (cf. Figure 1c) or may even grow across the interval (cf. Figure 1d). Then the analysis presented here breaks down, there is no distinct layer region, and a different approach must be used. The WKB method is appropriate for such problems and is presented in [11].]

3.2 Layer on the right. For the class of DDEs (2.1) with $a(x) < 0$ on $0 \le x \le 1$, a boundary layer occurs at $x = 1$ for ε and $\delta(\varepsilon)$ sufficiently small. A fascinating feature of this class of BVPs for DDEs with a negative shift having layer solutions on the right is

that the layer equation has a positive shift rather than a negative shift. This leads to a novel Laplace transform problem. Numerical solutions for the case $a(x) = -1$, $b(x) = -1$, f(x) $= 0, \phi(x) = 1$, $\gamma = -1$, and $\varepsilon = 0.01$ with $\tau = 0, 0.7$, and 1.5 are shown in Figure 3.

The outer solution is easily found to be

$$y(x;\varepsilon) = c \exp\left[-\int_0^x \frac{b(t)}{a(t)}\, dt\right] + O(\varepsilon) \quad as \quad \varepsilon \to 0, \tag{3.21}$$

on $0 < x < 1$ where the constant c is found by matching with the solution near $x = 0$. Attempting a layer solution near $x = 0$, the coefficient of the exponential term is $\phi(0)$ and corresponds to the boundary condition at $x = 0$. However, this outer solution is not strictly valid near $x = 0$ because of the shifted term and the interval condition (2.2). It can be shown that the deviation of the outer solution from the exact solution in an $O(\varepsilon)$-neighborhood of $x = 0$ is $O(\varepsilon)$. Note that this $O(\varepsilon)$ deviation does not correspond to the $O(\varepsilon)$ correction in the outer solution (3.21).

For the boundary layer at $x = 1$, introduce new independent and dependent variables

$$\hat{x} \equiv \frac{1-x}{\varepsilon}, \quad \hat{y}(\hat{x};\varepsilon) \equiv y(1 - \varepsilon\hat{x};\varepsilon), \tag{3.22}$$

where it is assumed that

$$\hat{y}(\hat{x};\varepsilon) \sim \sum_{j=0}^{\infty} \hat{y}_j(\hat{x})\varepsilon^j \quad \text{as} \quad \varepsilon \to 0. \tag{3.23}$$

Thus (2.1) becomes

$$\hat{y}''(\hat{x};\varepsilon) - a(1-\varepsilon\hat{x})\hat{y}'(\hat{x}+\tau;\varepsilon) + \varepsilon b(1-\varepsilon\hat{x})\hat{y}(\hat{x};\varepsilon) = 0, \tag{3.24}$$

recall $\delta(\varepsilon) \equiv \tau\varepsilon$. Setting $\varepsilon = 0$ in (3.24) yields the equations for the leading-order solution

$$\hat{y}_0''(\hat{x}) - a(1)\hat{y}_0'(\hat{x}+\tau) = 0, \tag{3.25}$$

on $0 < \hat{x} < \infty$ with conditions

$$\hat{y}_0(0) = \gamma, \quad \lim_{\hat{x}\to\infty} \hat{y}_0(\hat{x}) = \exp\left[-\int_0^1 \frac{b(t)}{a(t)}\, dt\right] \equiv \Phi. \tag{3.26}$$

Without loss of generality, set $a(1) = -1$. Integrating (3.25) once yields

$$\hat{y}_0'(\hat{x}) + \hat{y}_0(\hat{x} + \tau) = \Phi, \quad 0 < \hat{x} < \infty. \tag{3.27}$$

In contrast to (3.14), $\hat{y}_0'(0)$ cannot be determined here because of the positive shift term.

Apply the Laplace transform $\hat{Y}_0(s) = \mathcal{L}[\hat{y}_0(\hat{x})]$ to (3.27) where

$$\mathcal{L}[\hat{y}_0(\hat{x} + \tau)] = \int_0^\infty \hat{y}_0(t + \tau)e^{-ts}dt = e^{\tau s}\hat{Y}_0(s) - e^{\tau s}\int_0^\tau \hat{y}_0(t)e^{-ts}dt, \tag{3.28}$$

yielding

$$\hat{Y}_0(s) = \frac{\gamma + \frac{\Phi}{s} + e^{\tau s}\int_0^\tau \hat{y}_0(t)e^{-ts}ds}{s + e^{\tau s}}. \tag{3.29}$$

This does not provide an explicit representation for the Laplace transform since $\hat{y}_0(t)$ for $0 \le t \le \tau$ occurs on the right side and is not known. Such difficulties arise due to the positive shift term in the equation, cf. (3.27), and (4.10) for a mixed equation, i.e., with both negative and positive shift terms.

In Appendix 2.1, it is shown that for the exponential polynomial, $s + e^{\tau s}$ with $\tau > 0$, there is always one negative real root, s_0, with $-1 < s_0 < 0$, see Figure 4a, and all other complex conjugate roots are located in the right half s-plane for $0 < \tau < 3\pi/2$, see Figure 4b. Clearly the Laplace transform, $\hat{Y}_0(s)$, of $\hat{y}_0$ does not exist unless the numerator in (3.29) is zero at each root of the exponential polynomial to the right of some vertical line in the complex s-plane. Furthermore to match with the outer solution, there cannot be any

growing solutions and the Laplace transform, $\hat{Y}_0(s)$, must be analytic in the entire right-half plane. Thus the numerator in (3.29) must be zero at <u>all</u> the roots in the right-half s-plane. Consider the ansatz

$$\hat{y}_0(\hat{x}) = \Phi + (\gamma - \Phi)e^{s_0\hat{x}} \tag{3.30}$$

where s_0 is the negative real root. This ansatz satisfies the boundary condition at $\hat{x} = 0$ and the matching condition as $\hat{x} \to \infty$. It also satisfies (3.29) which is easily verified by direct substitution and comparing the two sides of the equation. Amazingly the numerator on the right-side of (3.29) is zero at each complex root of $P(s; -\tau)$ and hence the Laplace transform $\hat{Y}_0(s)$ is indeed analytic for $\mathrm{Re}\, s > s_0$.

To verify the accuracy of the layer solution (3.30), the values of $\hat{y}_0'(0)$ are compared with the exact numerical slopes at $x = 1$ for the examples corresponding to Figure 3. The slope is given by $\hat{y}_0'(0) = s_0(\gamma - \Phi)$. The outer solution in Figure 3 is approximated by $y(x;\varepsilon) \sim \epsilon^{-x}$ so $\Phi = \epsilon^{-1}$ and $\hat{y}_0'(0) = -s_0(1 + \epsilon^{-1})$. For $\tau = 0.7$ and 1.5, the real roots are $s_0 = -0.639$ and -0.485, respectively. Thus $\hat{y}_0'(0) = 0.874$ and 0.663 for $\tau = 0.7$ and 1.5, respectively. The exact numerical values are 0.869 and 0.669, respectively (cf. Figure 3).

4. Layer behavior for Model Problem 2. For the class of DDEs (2.3) with $\alpha(x) + \omega(x) + \beta(x) < 0$ on $0 \le x \le 1$, there are layers at both $x = 0$ and $x = 1$ for $\varepsilon, \delta(\varepsilon)$, and $\eta(\varepsilon)$ sufficiently small. The BVP is analyzed by introducing boundary layers at the ends. In particular, we carry out the analysis with the assumptions that both δ and η are of $O(\varepsilon)$; specifically we assume $\delta(\varepsilon) \equiv \tau\varepsilon$ and $\eta(\varepsilon) \equiv \mu\varepsilon$. Because there are no first-order derivative terms, the shifts in the undifferentiated terms have significant effects and contribute to the leading-order solution in the layer regions.

In this section, we begin with a short discussion of the outer solution and then derive the Laplace transforms for the leading-order solutions at $x = 0$ and $x = 1$. However, it is convenient to discuss the leading-order solutions separately for the case of $\beta(x) \equiv 0$, i.e., with only a negative shift term, and then the case of $\beta(x) \neq 0$, i.e., the equation of mixed type.

An analysis of the layer equations with both δ and η of $O(\varepsilon)$ indicates the solution is a power series expansion in ε, thus the outer solution is assumed to have the form

$$y(x;\varepsilon) \sim \sum_{j=0}^{\infty} y_j(x)\varepsilon^j \qquad \varepsilon \to 0. \tag{4.1}$$

After expanding out the shift terms in (2.3) for small $\delta(\varepsilon)$ and $\eta(\varepsilon)$, and then substituting (4.1) into the result, one obtains the leading-order solution

$$y_0(x) = \frac{f(x)}{\alpha(x) + \omega(x) + \beta(x)} , \tag{4.2}$$

and the sequence of higher-order corrections

$$y_1(x) = \frac{\tau\alpha(x) - \mu\beta(x)}{\alpha(x) + \omega(x) + \beta(x)}\, y_0'(x) , \tag{4.3}$$

$$y_2(x) = \frac{\tau\alpha(x) - \mu\beta(x)}{\alpha(x) + \omega(x) + \beta(x)}\, y_1'(x) - \frac{1}{2}\frac{\tau^2\alpha(x) + \mu^2\beta(x)}{\alpha(x) + \omega(x) + \beta(x)} y_0''(x) , \tag{4.4}$$

etc.

For the boundary layer at $x = 0$, introduce the new variables

$$\tilde{x} \equiv \frac{x}{\varepsilon} , \quad \tilde{y}(\tilde{x};\varepsilon) \equiv y(\varepsilon\tilde{x};\varepsilon) , \tag{4.5}$$

so (2.3) becomes

$$\tilde{y}''(\tilde{x};\varepsilon) + \alpha(\varepsilon\tilde{x})\tilde{y}(\tilde{x} - \tau;\varepsilon) + \omega(\varepsilon\tilde{x})\tilde{y}(\tilde{x};\varepsilon) + \beta(\varepsilon\tilde{x})\tilde{y}(\tilde{x} + \mu;\varepsilon) = f(\varepsilon\tilde{x}). \tag{4.6}$$

Assuming the layer solution at $x = 0$ has the expansion

$$\tilde{y}(\tilde{x},\varepsilon) \sim \sum_{j=0}^{\infty} \tilde{y}_j(\tilde{x})\varepsilon^j \qquad \text{as } \varepsilon \to 0, \tag{4.7}$$

the leading-order equation is given by

$$\tilde{y}_0''(\tilde{x}) + \alpha(0)\tilde{y}_0(\tilde{x}-\tau) + \omega(0)\tilde{y}_0(\tilde{x}) + \beta(0)\tilde{y}_0(\tilde{x}+\mu) = f(0), \tag{4.8}$$

on $0 \le \tilde{x} < \infty$. Since $f(0)$ is a constant, it is convenient to eliminate it by introducing the new variable

$$\tilde{u}(\tilde{x}) \equiv \frac{\tilde{y}_0(\tilde{x}) - \frac{f(0)}{\alpha(0)+\omega(0)+\beta(0)}}{1 - \frac{f(0)}{\alpha(0)+\omega(0)+\beta(0)}} \tag{4.9}$$

then $\tilde{u}(\tilde{x})$ satisfies the homogeneous equation

$$\tilde{u}''(\tilde{x}) + \alpha(0)\tilde{u}(\tilde{x}-\tau) + \omega(0)\tilde{u}(\tilde{x}) + \beta(0)\tilde{u}(\tilde{x}+\mu) = 0\ , \tag{4.10}$$

on $0 < \tilde{x} < \infty$, $\tilde{u}(0) = 1$, and $\lim_{\tilde{x}\to\infty} \tilde{u}(\tilde{x}) = 0$. Apply the Laplace transform $\tilde{U}(s) \equiv \mathcal{L}[\tilde{u}(\tilde{x})]$ to (4.10) to obtain

$$\tilde{U}(s) = \frac{s + \tilde{u}'(0) + \frac{\alpha(0)}{s}(e^{-\tau s} - 1) + \beta(0)e^{\mu s}\int_0^{\mu} \tilde{u}(t)e^{-ts}\,dt}{s^2 + \alpha(0)e^{-\tau s} + \omega(0) + \beta(0)e^{\mu s}} \tag{4.11}$$

where it is assumed that $\phi(x) = 1$. Again, cf. (3.29), this is not an explicit representation for the Laplace transform since $\tilde{u}(t)$ for $0 \le t \le \mu$ occurs on the right side and is not known.

Before analyzing this Laplace transform solution, we carry out the Laplace transform solution for the layer at $x = 1$. Introduce the new variables

$$\hat{x} \equiv \frac{1-x}{\varepsilon}, \quad \hat{y}(\hat{x};\varepsilon) \equiv y(1-\varepsilon\hat{x};\varepsilon)\ , \tag{4.12}$$

so (2.3) becomes

$$\hat{y}''(\hat{x};\varepsilon) + \alpha(1-\varepsilon\hat{x})\hat{y}(\hat{x}+\tau;\varepsilon) + \omega(1-\varepsilon\hat{x})\hat{y}(\hat{x};\varepsilon)$$

(4.13)

$$+ \beta(1-\varepsilon\hat{x})\hat{y}(\hat{x}-\eta;\varepsilon) = f(1-\varepsilon\hat{x}),$$

where the main difference compared to (4.6) is that here the left shift has become a right shift and vice versa.

Assuming that

$$\hat{y}(\hat{x};\varepsilon) \sim \sum_{j=0}^{\infty} \hat{y}_j(\hat{x})\varepsilon^j \qquad \text{as} \quad \varepsilon \to 0, \tag{4.14}$$

the equation for the leading-order solution is

$$\hat{y}_0''(\hat{x}) + \alpha(1)\hat{y}_0(\hat{x}+\tau) + \omega(1)\hat{y}_0(\hat{x}) + \beta(1)\hat{y}_0(\hat{x}-\eta) = f(1) \tag{4.15}$$

on $0 < \hat{x} < \infty$. Again, the forcing term $f(1)$ can be eliminated by defining

$$\hat{u}(\hat{x}) \equiv \frac{\hat{y}_0(\hat{x}) - \frac{f(1)}{\alpha(1)+\omega(1)+\beta(1)}}{\psi(1) - \frac{f(1)}{\alpha(1)+\omega(1)+\beta(1)}} \tag{4.16}$$

where $\psi(1)$ is the value $y(1;\varepsilon)$ for $\beta(x) \neq 0$ and is set equal to γ if $\beta(x) \equiv 0$. Thus (4.15) becomes

$$\hat{u}''(\hat{x}) + \alpha(1)\hat{u}(\hat{x}+\tau) + \omega(1)\hat{u}(\hat{x}) + \beta(1)\hat{u}(\hat{x}-\eta) = 0, \tag{4.17}$$

on $0 < \hat{x} < \infty$, $\hat{u}(0) = 1$, and $\lim_{\hat{x}\to\infty} \hat{u}(\hat{x}) = 0$. Apply the Laplace transform $\hat{U}(s) \equiv \mathcal{L}[\hat{u}(\hat{x})]$ to (4.17) to obtain

$$\hat{U}(s) = \frac{s + \hat{u}'(0) + \alpha(1)e^{\tau s}\int_0^{\tau} \hat{u}(t)e^{-ts}dt + \frac{\beta(1)}{s}(e^{-\mu s} - 1)}{s^2 + \alpha(1)e^{\tau s} + \omega(1) + \beta(1)e^{-\mu s}} \tag{4.18}$$

where it is assumed that $\hat{u}(\hat{x}) = 1$ for $-\mu \leq \hat{x} \leq 0$. Again an integral over $\hat{u}(t)$ for $0 \leq t \leq \tau$ occurs on the right side and is not known.

4.1. Case of $\beta(\mathbf{x}) \equiv 0$. Before considering the problem of mixed type with both negative and positive shifts, it is simpler to treat the case with $\beta(x) \equiv 0$. Numerical examples are shown in Figures 5a,b,c,d with $\alpha(x) = -2, \omega(x) = -1, f(x) = 1, \gamma = 0$, and $\varepsilon = 0.01$ for $\tau = 0$, 1.5, 3, 5, respectively. Although Figures 5a and 5b show layer behavior, that structure is completely destroyed in Figures 5c and 5d where oscillations occur all across the interval. These latter oscillatory solutions are treated in the companion paper [11]. For $\beta(x) \equiv 0$, (4.11) reduces to

$$\tilde{U}(s) = \frac{1}{s} + \frac{\tilde{u}'(0)s - \alpha(0) - \omega(0)}{s\left[s^2 + \alpha(0)e^{-\tau s} + \omega(0)\right]}. \tag{4.19}$$

The determination of the inversion of $\tilde{U}$ requires a knowledge of the root structure of the exponential polynomial, $Q(s;\tau) = s^2 + \alpha(0)e^{-\tau s} + \omega(0)$. In Appendix 2.2, it is shown that for the special case $\omega(0) = -1$, there is one and only one positive real root for $0 < \tau < \infty$, say $s = s_R$, see Figure 6a. For sufficiently small τ (e.g., $0 < \tau \leq 0.5044$ for $\alpha(0) = -2$ and $\omega(0) = -1$), there are two negative real roots, see Figure 6a, and all complex conjugate roots are in the left-half s-plane for $0.5044 < \tau < \pi$.

In order to satisfy the matching condition, $\lim_{\tilde{x}\to-\infty} \tilde{u}(\tilde{x}) = 0$, there cannot be any contribution from the real positive root, s_R. Thus the numerator in the second term on the right side of (4.19) must equal zero at $s = s_R$ which then determines $\tilde{u}'(0)$, namely

$$\tilde{u}'(0) = \frac{\alpha(0) + \omega(0)}{s_R}. \tag{4.20}$$

Therefore, only the poles in the left-hand s-plane contribute to the solution $\tilde{u}(\tilde{x})$ which can be written in the form

$$\tilde{u}(\tilde{x}) = c_0 e^{s_0\tilde{x}} + c_1 e^{s_1\tilde{x}} + \sum_{n=2}^{\infty}(c_n e^{s_n\tilde{x}} + \overline{c}_n e^{\overline{s}_n\tilde{x}}), \tag{4.21}$$

where the terms involving s_0 and s_1 correspond to the contributions from the two real negative roots for sufficiently small τ. As τ is increased, s_0 and s_1 coalesce and split off into a complex conjugate pair as τ is increased, so let $s_0 = \bar{s}_1$ and $c_0 = \bar{c}_1$. Taking the Laplace transform of (4.21) and inserting into the left side of (4.19) yields (using (4.20))

$$\frac{c_0}{s-s_0} + \frac{c_1}{s-s_1} + \sum_{n=2}^{\infty}\left(\frac{c_n}{s-s_n} + \frac{\bar{c}_n}{s-\bar{s}_n}\right) = \frac{1}{s} + \frac{[\alpha(0)+\omega(0)]\left(\frac{s}{s_R}-1\right)}{s[s^2+\alpha(0)e^{-\tau s}+\omega(0)]}, \tag{4.22}$$

so that evaluation of the residues at the roots of $Q(s;\tau)$ yields

$$c_n = \frac{[\alpha(0)+\omega(0)]\left(\frac{s_n}{s_R}-1\right)}{s_n\,(2s_n - \tau + \tau\, s_n^2)}, \quad n = 0, 1, 2, \ldots . \tag{4.23}$$

For the examples shown in Figures 5a and 5b, $s_R = \sqrt{3}$ and 1.1620 for $\tau = 0$ and 1.5, respectively, so that using (4.9) $\tilde{y}'(0) \simeq -2.306$ and -3.4423, respectively. The corresponding values obtained from the numerical computations (i.e., for Figures 5a and 5b) are (using (4.9)) $\tilde{y}_0'(0) \simeq -2.3094$ and -3.4425, respectively. The leading-order results are remarkably accurate. As noted earlier, the solutions shown in Figures 5c and 5d cannot be treated using the method described here. See [11] for treatment of these cases using a WKB method.

For the boundary layer at $x = 1$ (with $\beta(x) = 0$), the exponential polynomial is given by

$$s^2 + \alpha(1)e^{\tau s} + \omega(1) = 0. \tag{4.24}$$

Results on the roots of this equation are given in Appendix 2.2 corresponding to $Q(s;-\tau)$ with $\tau \geq 0$. Thus for small τ there is one negative real root in the left-half plane and two positive real roots in the right-half plane, see Figure 6a (with $\tau < 0$). For larger values

of τ, all complex conjugate roots are in the right-half s-plane, see Figure 6c for s_1 and $\bar{s}_1$ (with $\tau < 0$).

The ansatz in this case is that the solution to the leading-order layer solution consists of a contribution only from the negative real root, say $s = s_0$, namely

$$\hat{u}(\hat{x}) = e^{s_0 \hat{x}}, \tag{4.25}$$

which satisfies the boundary condition at $\hat{x} = 0$ and the matching condition with the outer solution. Thus $\hat{U}(s) = (s - s_0)^{-1}$ and (4.18) becomes

$$\frac{1}{s - s_0} = \frac{s + s_0 + \frac{\alpha(1)}{s - s_0}\left(e^{\tau s} - e^{\tau s_0}\right)}{s^2 + \alpha(1)e^{\tau s} + \omega(1)} \tag{4.26}$$

which reduces to an identity when $s_0^2 + \alpha(1)e^{\tau s_0} + \omega(1) = 0$ is used. Thus (4.25) is the exact leading-order solution and therefore the residues at all poles in the right-half plane are zero. Using (4.16), the leading-order solution is given by

$$\hat{y}_0(\hat{x}) = \frac{f(1)}{\alpha(1) + \omega(1)} + \left[\gamma - \frac{f(1)}{\alpha(1) + \omega(1)}\right] e^{s_0 \hat{x}}. \tag{4.27}$$

For the numerical example shown in Figures 5a and 5b, the leading-order layer solution at $x = 1$ is given by $\hat{y}_0(\hat{x}) = \left(4e^{s_0 \hat{x}} - 1\right)/3$. Note that $Q(-s; \tau) = Q(s; -\tau)$, therefore s_0 is the negative of the positive real root, s_R, obtained in Appendix 2.2. Thus $s_0 \simeq -\sqrt{3}$ and -1.1620 and $\hat{y}_0'(0) \simeq -2.3094$ and -1.5493 for $\tau = 0$ and 1.5, respectively. The numerical results give $\hat{y}'(0) \simeq -2.3094$ and 1.5366, respectively. The result for $\tau = 0$ is very close but the value for $\tau = 1.5$ is not as good as might have been expected considering the excellent agreement in the layer at $x = 0$.

4.2. Case with $\beta(x) \neq 0$ - equations of mixed type. When $\beta(x)$ and $\eta(x)$ are not zero with η small, there are still layers at $x = 0$ and at $x = 1$ provided $\alpha(x) + \omega(x) + \beta(x) <$

0. Numerical examples of this type of solution are plotted in Figures 7a,b for $\omega(x) = -1$, $f(x) = 1$, $\phi(x) = 1 = \psi(x)$, $\varepsilon = 0.01$ and setting $\alpha(x) = 0.25 = \beta(x)$ with $\tau = 0.7$ and $\mu = 0.5$, and $\alpha(x) = -2 = \beta(x)$ with $\tau = 1.5$ and $\mu = 0.7$, respectively.

When $\beta(x) \neq 0$, the functions $\tilde{u}$ and $\hat{u}$ occur in the integrals on the right sides of the Laplace transform equations (4.11) and (4.18), respectively. For the layer at $x = 0$, the ansatz (4.21) is assumed for $\tilde{u}(\tilde{x})$. For the parameter values corresponding to the solution plotted in Figure 7a, $c_0 \equiv 0$ and s_1 is the negative real root of

$$R(s;\tau;\mu) \equiv s^2 + \alpha e^{-\tau s} + \omega + \beta e^{\mu s} = 0. \tag{4.28}$$

see Figure 8a. The quantities s_n and $\overline{s}_n$ are the complex conjugate roots in the left-hand s-plane. For the parameter values corresponding to the solution plotted in Figure 7b, $s_0 = \bar{s}_1$ and $c_0 = \bar{c}_1$, see Figure 8b. The structure of the roots of $R(s;\tau;\mu) = 0$ is very different from that with $\beta(x) \equiv 0$, cf. Appendices 2.2 and 2.3. In particular there are infinitely many complex roots in both the left and right halves of the complex s-plane, cf. Figures 8a and b.

Substituting (4.21) into (4.11) yields the equation

$$\begin{aligned} &\frac{c_0}{s-s_0} + \frac{c_1}{s-s_1} + \sum_{n=2}^{\infty}\left(\frac{c_n}{s-s_n} + \frac{\overline{c}_n}{s-\overline{s}_n}\right) \\ &= \frac{1}{s} + \frac{1}{s\left[s^2 + \omega(0) + \alpha(0)e^{-\tau s} + \beta(0)e^{\mu s}\right]} \cdot \Bigg\{ \tilde{u}'(0)s - \alpha(0) - \omega(0) - \beta(0)e^{\mu s} \\ &\quad + \beta(0)s\Bigg\{ \left(e^{\mu s} - e^{\mu s_0}\right)\frac{c_0}{s-s_0} + \left(e^{\mu s} - e^{\mu s_1}\right)\frac{c_1}{s-s_1} \\ &\quad + \sum_{n=2}^{\infty}\left[\left(e^{\mu s} - e^{\mu s_n}\right)\frac{c_n}{s-s_n} + \left(e^{\mu s} - e^{\mu \overline{s}_n}\right)\frac{\overline{c}_n}{s-\overline{s}_n}\right]\Bigg\}\Bigg\}, \end{aligned} \tag{4.29}$$

where s is arbitrary. Although this equation is similar to (4.22), there are two major differences. Firstly, $\tilde{u}'(0)$ is not known and, secondly, the $c_n's$ also occur on the right side and cannot be solved for individually as was the case in (4.22) leading to (4.23). Thus $\tilde{u}'(0)$ and a doubly infinite set of coefficients, c_n and $\overline{c}_n$, are to be determined from (4.29) which is an identity in s.

To generate a sequence of infinitely many linear equations for these unknowns, there is, unfortunately, neither an obvious choice for the values of s nor is there an algorithm for solving the resulting system of equations. Our procedure was to choose a sequence of values of s and then the system of equations was truncated to a finite system. Then the inversion of the coefficient matrix is done carefully because it becomes ill-conditioned with relatively few equations, e.g., $n > 5$ in the cases of the solutions plotted in Figures 7. With these caveats, computations for the solutions in Figure 7 yielded the slope $\tilde{u}'(0)$ and the first four coefficients, $c_n, n = 1, 2, 3, 4$. The remaining $c_n's$ are small. Furthermore, there is a constraint on the coefficients which was used as a check. From (4.21), the sum of the coefficients, i.e., at $\tilde{x} = 0$, must equal $\tilde{u}(0) = 1$, thus

$$\sum_{n=1}^{\infty}(c_n + \overline{c}_n) = 1. \tag{4.30}$$

For the solution plotted in Figure 7a, using four terms in (4.21), i.e., $n = 1, ..., 4$, with (4.9),the approximation for $\tilde{y}'(0)$ is -2.0741 whereas the numerically computed value using COLSYS is -2.0742. The sum of the first four coefficients on the left side of (4.30) was equal to 0.99812. Because of the rapid decay of the exponential terms in (4.21) as $\tilde{x}$ is increased, to the right of $x \simeq 0.01$ one term suffices to give an approximation to the solution accurate to four significant figures.

For the solution plotted in Figure 7b, four terms in (4.21) yield the approximation $\tilde{y}'(0) \simeq -2.6852$ whereas the COLSYS generated value is -2.6849. The sum of the first four coefficients on the left side of (4.30) was equal to 0.99300. One term in the approximate solution (4.21) suffices to the right of $x \simeq 0.04$ for five significant figures of accuracy.

Computations for the layers at $x = 1$ can be carried out similarly.

Appendix 1. Numerical computations. In this appendix we discuss the algorithm used to compute the numerical solutions presented in this paper. These computations provided numerical confirmation of the accuracy of the leading-order solutions derived here using singular perturbation methods. Our previous usage of COLSYS, see [1] and [7], permitted us to collapse the problem on the interval $0 \leq x \leq \ell, \ell = 1.5$ or 2, to a shorter interval either equal to the shift length or to half the shift length. With small shifts, collapsing the interval is impractical. Instead we devised an iterative scheme using COLSYS at each step or used a finite difference method on the full DDE.

The iteration algorithm used to solve Model Problem 1 consisted of solving a forced ODE at each step. The ODE consists of (2.1) with the shifted derivative term replaced by an unshifted derivative term and forced by the difference between the values of the unshifted and shifted derivative terms at the previous step. Specifically, replace (2.1) by

$$\varepsilon y_n''(x;\varepsilon) + a(x)y_n'(x;\varepsilon + b(x)y_n(x;\varepsilon) \tag{A.1.1}$$

$$= f(x) + a(x)[y_{n-1}'(x;\varepsilon) - y_{n-1}'(x-\delta(\varepsilon);\varepsilon)], \quad n = 1, 2, \ldots .$$

If the iteration converges, i.e., $y_n = y_{n-1}$, then this equation collapses to (2.1). For Model Problem 2, the shifted terms are approximated by the first two terms of a Taylor series.

Thus replace (2.3) by

(*A*.1.2)

$$\varepsilon^2 y_n''(x;\varepsilon) + \alpha(x)[y_n(x;\varepsilon) - \delta(\varepsilon)y_n'(x;\varepsilon)] + \omega(x)y_n(x;\varepsilon) + \beta(x)[y_n(x;\varepsilon) + \eta(\varepsilon)y_n'(x;\varepsilon)]$$

$$= f(x) + \alpha(x)[y_{n-1}(x;\varepsilon) - \delta(\varepsilon)y_{n-1}'(x;\varepsilon) - y_{n-1}(x - \delta(\varepsilon);\varepsilon)]$$

$$+\beta(x)[y_{n-1}(x;\varepsilon) + \eta(\varepsilon)y_{n-1}'(x;\varepsilon) - y_{n-1}(x + \eta(\varepsilon);\varepsilon)], \quad n = 1, 2, \ldots .$$

Again if $y_n = y_{n-1}$, this equation collapses to (2.3).

For both (A.1.1) and (A.1.2), at step n, COLSYS is used to determine $y_n(x;\varepsilon)$ where $y_{n-1}(x;\varepsilon)$ is known, and this procedure is iterated. The initial guess $y_0(x;\varepsilon)$ was taken to be the solution of the problem with $\delta(\varepsilon) \equiv 0$ (and $\eta(\varepsilon) \equiv 0$). The difference $\max_{x\in[0,1]} |y_n(x;\varepsilon) - y_{n-1}(x;\varepsilon)|$ is computed at each iteration and when this number is sufficiently small, the computation is stopped and the numerical solution is assumed to have converged. Typically there were of $O(10)$ iterations for both cases when $\varepsilon = 0.01$. It should be noted, however, that this iteration scheme worked well provided the shifts were not too large.

In some cases where the shift was too large or because of space and precision limitations, COLSYS did not compute a stabilized solution, i.e., with $|y_n - y_{n-1}|$ sufficiently small. This was particularly true for solutions which contained oscillations where the iteration scheme did not work when $\delta = O(\varepsilon)$ [also see [11]]. In these cases a finite difference method with a standard three-point centered difference scheme having approximately 1000 uniformly distributed points was implemented using Gauss elimination. The finite difference computations also served to check the COLSYS iterations when they did converge.

However, because of the shifted derivative term in (2.1), the discontinuity in the derivative at $x = 0$ induces a discontinuity in the second derivative term at $x = \delta(\varepsilon)$.

Therefore at $x = \delta$, we impose an interface continuity condition on the one-sided derivatives

$$y'(\delta^-) = y'(\delta^+). \tag{A.1.3}$$

For example, $y'(\delta^-)$ was given by the three-point formula (with $h = \Delta x$):

$$y'_L(\delta^-) \simeq \frac{3y(\delta) - 4y(\delta - h) + y(\delta - 2h)}{2h}. \tag{A.1.4}$$

The error in the solution near $x = 0$ was significant if the presence of the jump in y'' was not accounted for in the finite difference scheme. The derivative of the solution at $x = 0$ had an error of approximately 5%. No efforts were made to optimize this numerical algorithm.

Appendix 2. Roots of exponential polynomials. Numerical evaluation of the leading-order layer solutions obtained using the Laplace transform requires values of the roots of several exponential polynomials, see Bellman and Cooke [2]. In this appendix, the root structure of these exponential polynomials is examined and asymptotic formulas are given for some of the roots.

1. Roots of $\mathbf{P(s;\tau) \equiv s + e^{-\tau s}}$. The exponential polynomial

$$P(s;\tau) \equiv s + e^{-\tau s}, \quad \tau \text{ real}, \ 0 \le \tau < \infty, \tag{A.2.1}$$

arises in the Laplace transform solution of (2.1) in the layer region at $x = 0$ for $a(x) > 0$. For $a(x) < 0$, the layer occurs at $x = 1$ and it sufficies to examine $P(s;-\tau) = s + e^{\tau s}$ for $0 \le \tau < \infty$. Thus the roots of $P(s;\tau)$ will be examined for $-\infty < \tau < \infty$.

First consider the real roots of $P(s;\tau)$, say $s = \sigma$. Obviously, if $\tau = 0$, then $s = -1$. For $\tau \neq 0$, a simple analysis of $P(s;\tau)$ shows that as τ increases from zero, there are two

real roots, one increasing from $-\infty$ and the other root starting at $s = -1$ and decreasing (see Figure 2a). These roots coalesce at $s = -e$ when $\tau = 1/e$. As τ increases further, these roots split into a complex conjugate pair and there are only complex roots for $\tau > 1/e$ (see Figure 2b). These are discussed below. For τ decreasing from zero, the real root at $s = -1$ increases and asymptotes to $s = 0$ as $\tau \to -\infty$. Thus for $s + e^{s\tau}$, there is always one negative real root for $\tau \geq 0$. (see Figure 4b).

For the complex conjugate roots of $P(s;\tau)$, let $s = \sigma + i\rho$, σ, ρ real. Then $P(s;\tau) = 0$ can be rewritten as the set of coupled transcendental equations

$$\sigma = -e^{-\tau\sigma}\cos(\tau\rho), \tag{A.2.2}$$

$$\rho = e^{-\tau\sigma}\sin(\tau\rho). \tag{A.2.3}$$

First consider the case of pure imaginary roots, i.e., $\sigma = 0$, with $\tau > 0$. From (A.2.2), this requires

$$\rho = \frac{2m+1}{2\tau}\pi, \quad m = 0, 1, 2, \ldots, \quad \tau > 0. \tag{A.2.4}$$

It suffices to consider only $\rho > 0$ since the roots occur in complex conjugate pairs. Using (A.2.4) in (A.2.3) yields $\rho = \pm 1$ and $\rho = 1$ only if m is even. Thus all complex roots in the upper half plane cross the imaginary axis at $\rho = 1$ for values of τ given by

$$\tau = \frac{4n-3}{2}\pi, \quad n = 1, 2, \ldots, \tag{A.2.5}$$

where n identifies the root number. Note that the roots which were real for small τ correspond to the complex conjugate pair for $n = 1$ and crosses the imaginary axis at $\tau = \pi/2$.

For $\tau < 0$, a similar argument shows that the roots cross the imaginary axis at $\rho = 1$ for values of τ given by

$$\tau = -\frac{4n-1}{2}\pi, \quad n = 1, 2, \ldots , \tag{A.2.6}$$

where n is the root number.

Graphs of the first three complex roots of $s + e^{-\tau s}$ and $s + e^{\tau s}$ in the upper half plane are given in Figures 2b and 4b, respectively. Numerical values of τ are indicated on each curve. All complex roots asymptote to 0 as $\tau \to \infty$.

Equations (A.2.2) and (A.2.3) can be analyzed for large complex roots with $|\tau| = O(1)$. All complex conjugate roots are in the left-half (right-half) plane for values of $0 < \tau < \frac{\pi}{2}$ ($-\frac{3\pi}{2} < \tau < 0$). The asymptotic formulas for the nth complex root are (with $m = 4n - 3$ for $\tau > 0$ and $m = 4n - 1$ for $\tau < 0$)

$$\sigma_n \sim \frac{1}{\tau}\ell n\left(\frac{2|\tau|}{m\pi}\right) - \frac{2}{m^2\pi^2\tau}\left\{\left[\ell n\left(\frac{2|\tau|}{m\pi}\right)\right]^2 + 2\ell n\left(\frac{2|\tau|}{m\pi}\right)\right\}, \tag{A.2.7}$$

$$\rho_n \sim \frac{m\pi}{2|\tau|} + \frac{2}{m\pi|\tau|}\ell n\left(\frac{2|\tau|}{m\pi}\right), \tag{A.2.8}$$

with $n \to \infty$ through the positive integers. Although for a given τ, n must be chosen sufficiently large so that the formulas are valid, it is surprising that the above expansions for the complex roots are accurate to three significant figures even for $\tau = 1$ and $n = 2$, $s_2 \sim -2.062 + i7.592$ and the actual root is $s_2 = -2.062 + i7.588$ to four significant figures.

2. Roots of $\mathbf{Q(s;\tau) \equiv s^2 + \alpha e^{-\tau s} + \omega}$. The exponential polynomial $Q(s;\tau)$ contains three parameters, τ, α, and ω, and $Q(s;\tau) = 0$ can be rewritten as

$$s^2 = -\alpha\, e^{-\tau s} - \omega. \tag{A.2.9}$$

First, consider the case of real roots, say $s = \sigma$. Recall that for layer behavior, $\alpha + \omega < 0$, thus for $\tau = 0$, $\sigma = \pm\sqrt{-\alpha - \omega}$. For $-\infty < \tau < \infty$, a simple geometrical argument shows that there is always one real root and at most three real roots, see Figure 6a for the special case of $\alpha = -2$ and $\omega = -1$. For this special case, note that for $\tau > 0$, there is one and only one positive real root. The negative real roots for $\tau > 0$ coalesce at $\tau_0 = 0.5044$ and then split into a complex conjugate pair for $\tau > \tau_0$.

We restrict our attention to the case with $\omega = -1$ and study the complex roots of $Q(s;\tau)$, $s = \sigma + i\rho$, σ and ρ real. For $\alpha = -2$, a plot of the first three complex roots in the upper half plane is shown in Figure 6b. Numerical values of τ are indicated on each curve. Note that root 1 crosses the imaginary axis for $\tau = \pi$ and all other roots cross the imaginary axis for larger values of τ. In Figure 6c is shown a plot of the complex conjugate pair of roots designated s_1 and $\bar{s}_1$ for $|\tau| \geq 0.5044$, again with values of τ indicated on the curves.

Splitting $Q(s;\tau) = 0$ (with $\omega = -1$) into its real and imaginary parts gives

$$\sigma^2 - \rho^2 - 1 = -\alpha e^{-\tau\sigma}\cos(\tau\rho), \tag{A.2.10}$$

$$2\sigma\rho = \alpha e^{-\tau\sigma}\sin(\tau\rho). \tag{A.2.11}$$

An analysis of these equations can be carried out to determine an asymptotic approximation for the large complex conjugate roots. All large complex conjugate roots are given asymptotically by (with $m = 2n$ for $\alpha > 0$ and $m = 2n - 1$ for $\alpha < 0$)

(A.2.12)

$$\sigma_n \sim \frac{2}{\tau}\ell n\left(\frac{\sqrt{|\alpha|}|\tau|}{m\pi}\right) - \frac{4}{\pi^2 m^2 \tau}\left\{\left[\ell n\left(\frac{\sqrt{|\alpha|}|\tau|}{m\pi}\right)\right]^2 + 2\ell n\left(\frac{\sqrt{|\alpha|}|\tau|}{m\pi}\right) + \frac{\tau^2}{4}\right\},$$

$$\rho_n \sim \frac{m\pi}{|\tau|} + \frac{4}{\pi m|\tau|}\ell n\left(\frac{\sqrt{|\alpha||\tau|}}{m\pi}\right), \tag{A.2.13}$$

and by $\sigma - i\rho$ where n is the number of the complex root with $n \to \infty$ through the positive integers. Note that in the formula for σ_n, the $[\ell_n(\cdot)]^2$ term is dominant inside the braces; however, for moderate values of n the other two terms are of comparable magnitude and hence have been kept.

3. Roots of $\mathbf{R(s;\tau,\mu) \equiv s^2 + \alpha e^{-\tau s} + \omega + \beta e^{\mu s}}$. The exponential polynomial $R(s;\tau;\mu)$ contains five parameters, $\tau, \mu, \alpha, \omega$, and β, and $R(s;\tau;\mu)$ can be rewritten as

$$s^2 = -\alpha e^{-\tau s} - \omega - \beta e^{\mu s}. \tag{A.2.14}$$

First, consider the case of real roots, say $s = \sigma$. For layer behavior, $\alpha + \omega + \beta < 0$, thus for $\tau = 0 = \mu$, $\sigma = \pm\sqrt{-\alpha - \omega - \beta}$. For either $\tau = 0$ and $\mu > 0$ or $\tau > 0$, $\mu = 0$, a study of $R(s;\tau;\mu)$ reduces to a study of Q. If $\tau > 0$ and $\mu > 0$, then the study of R is more difficult. In Figure 8a, for the case $\alpha = 0.25 = \beta$, $\tau = 0.7$, and $\mu = 0.5$, there are two real roots, one positive and one negative. In Figures 8b, for the case $\alpha = -2 = \beta$, $\tau = 1.5$, and $\mu = 0.7$, there are no real roots but there is a complex conjugate pair with small negative real parts and small imaginary parts.

For the complex roots of R, with $\omega = -1$, let $s = \sigma + i\rho$, σ and ρ real. Note that in Figures 10a and 10b, the imaginary parts of the roots grow much more rapidly than the real parts.

Splitting R into its real and imaginary parts gives

$$\sigma^2 - \rho^2 - 1 + \alpha e^{-\tau\sigma}\cos(\tau\rho) + \beta e^{\mu\sigma}\cos(\mu\rho) = 0, \tag{A.2.15}$$

$$2\sigma\rho - \alpha e^{-\tau\sigma}\sin(\tau\rho) + \beta e^{\mu\sigma}\sin(\mu\rho) = 0. \tag{A.2.16}$$

The asymptotic behavior of the large complex conjugate roots is obtained by reducing the problem to (A.2.10) and (A.2.11) since either the term with $e^{-\tau\sigma}$ or with $e^{\mu\sigma}$ is exponentially small.

Acknowledgment. We thank Mr. James Bence and Mr. Perry Pow for ably carrying out the numerical computations for the figures.

REFERENCES

[1] U. Ascher and R. Russell, *Reformulation of boundary value problems in 'standard' form*, SIAM Rev., 23 (1981), pp. 238-254.

[2] R. Bellman and K.L. Cooke, *Differential-Difference Equations*, Academic Press, New York, 1963.

[3] C.M. Bender and S.A. Orszag, *Advanced Mathematical Methods for Scientists and Engineers*, McGraw-Hill, New York, 1978.

[4] K.L. Cooke and K.R. Meyer. *The condition of regular degeneration of singularly perturbed system of linear differential equations*, J. Math. Anal. Appl., 14 (1966), pp. 83-106.

[5] J. Kevorkian and J. Cole, *Perturbation Methods in Applied Mathematics*, Springer-Verlag, New York, 1981.

[6] P. Lagerstrom, *Matched Asymptotic Expansions*, Springer-Verlag, New York, 1989.

[7] C.G. Lange and R.M. Miura, *Singular perturbation analysis of boundary-value problems for differential-difference equations*, SIAM J. Appl. Math., 42 (1985), pp. 502-531.

[8] ———, *Singular perturbation analysis of boundary-value problems for differential-difference equations. II. Rapid oscillations and resonances*, SIAM J. Appl. Math., 45 (1985), pp. 687-707.

[9] ———, *Singular perturbation analysis of boundary-value problems for differential-difference equations. III. Turning point problems*, SIAM J Appl. Math., 45 (1985), pp. 708-734.

[10] ———, *Singular perturbation analysis of boundary-value problems for differential-difference equations. IV. A nonlinear example with layer behavior*, Studies in Appl. Math., 84 (1991), pp. 231-273.

[11] ———, *Singular perturbation analysis of boundary-value problems for differential-difference equations. VI. Small shifts with rapid oscillations*, this Journal, this issue, pp. .

[12] R.M. Miura and C.G. Lange, *Particular solutions of forced generalized Airy equations*, J. Math. Anal. Appl., 109 (1985), pp. 303-310.

[13] R.E. O'Malley, *On the asymptotic solution of initial problems for differential equations with small delays*, SIAM J. Math. Anal., 2 (1971), pp. 259-268

[14] ———, *Introduction to Singular Perturbations*, Academic Press, New York, 1974.

[15] D.R. Smith, *Singular Perturbation Theory*, Cambridge University Press, Cambridge, 1985.

[16] R.B. Stein, *A theoretical analysis of neuronal variability*, Biophys. J., 5 (1965), pp. 173-194.

[17] H.C. Tuckwell, *On the first-exit time problem for temporally homogeneous Markov processes*, J. Appl. Prob., 13 (1976), pp. 39-48.

[18] ———, *Introduction to Theoretical Neurobiology*, Volume 2, Cambridge University Press, Cambridge, 1988.

[19] A.B. Vasil'eva, *Asymptotic solutions of differential-difference equations in the case of a small deviation in the argument*, USSR Comp. Math. Math. Phys., 2 (1962), pp. 869-893.

[20] W.J. Wilbur and J. Rinzel, *An analysis of Stein's model for stochastic neuronal excitation*, Biol. Cybern., 45 (1982), pp. 107-114.

FIGURE CAPTIONS

Figure 1. Graphs of numerical solutions of BVP (2.1) - (2.2) for $a(x) = 1$, $b(x) = 1$, $f(x) = 0$, $\phi(x) = 1$, $\gamma = 1$, and $\varepsilon = 0.01$. Figures 1a, 1b, 1c, and 1d correspond to the shift $\delta(\varepsilon) = \tau\varepsilon$ with $\tau = 0,\ 0.7,\ 1.5,\ 2.5$, respectively.

Figure 2. Graphs of the roots of the exponential polynomial $s + e^{-s\tau} = 0$. The real roots for $0 \leq \tau \leq 1/e$ are shown in Figure 2a. Three complex roots, $s = \sigma + i\rho$, in the upper half plane with values of τ given along the curves are shown in Figure 2b.

Figure 3. Graphs of numerical solutions of BVP (2.1) - (2.2) for $a(x) = -1$, $b(x) = -1$, $f(x) = 0$, $\phi(x) = 1$, $\gamma = -1$, and $\varepsilon = 0.01$. The three curves correspond to the shift $\delta(\varepsilon) = \tau\varepsilon$ with $\tau = 0,\ 0.7,\ 1.5$, respectively.

Figure 4. Graphs of the roots of the exponential polynomial $s + e^{s\tau} = 0$. The real root for $0 \leq \tau \leq 100$ is shown in Figure 4a. Three complex roots, $s = \sigma + i\rho$, in the upper half plane with values of τ given along the curves are shown in Figure 4b.

Figure 5. Graphs of numerical solutions of BVP (2.3) - (2.4) for $\alpha(x) = -2$, $\omega(x) = -1$, $\beta(x) = 0$, $f(x) = 1$, $\phi(x) = 1$, $\gamma = 0$, and $\varepsilon = 0.01$. Figures 5a, 5b, 5c, and 5d correspond to the shift $\delta(\varepsilon) = \tau\varepsilon$ with $\tau = 0,\ 1.5,\ 3,\ 5$, respectively. The insert in Figure 5d shows the oscillations continue all the way to the origin.

Figure 6. Graphs of the roots of the exponential polynomial $s^2 - 1 - 2e^{-s\tau} = 0$. The real roots are shown in Figure 6a. Three complex roots in the upper half plane, $s = \sigma + i\rho$, with values of τ given along the curves are shown in Figure 6b. Figure 6c shows one complex root for both negative and positive values of τ with $0.5044 \leq |\tau| < \infty$.

Figure 7. Graphs of numerical solutions of BVP (2.3) - (2.4) for $\omega(x) = -1$, $f(x) = 1$, $\phi(x) = 1 = \psi(x)$, and $\varepsilon = 0.01$. Figure 7a corresponds to $\alpha(x) = 0.25 = \beta(x)$ with $\tau = 0.7$ and $\mu = 0.5$, and Figure 7b corresponds to $\alpha(x) = -2 = \beta(x)$ with $\tau = 1.5$ and $\mu = 0.7$.

Figure 8. Graphs of the complex roots, $s = \sigma + i\rho$, of the exponential polynomial $s^2 + \alpha e^{-s\tau} - 1 + \beta e^{\mu s} = 0$. Figure 8a corresponds to $\alpha(x) = 0.25 = \beta(x)$ with $\tau = 0.7$ and $\mu = 0.5$, and Figure 8b corresponds to $\alpha(x) = -2 = \beta(x)$ with $\tau = 1.5$ and $\mu = 0.7$.

FIGURE 1a

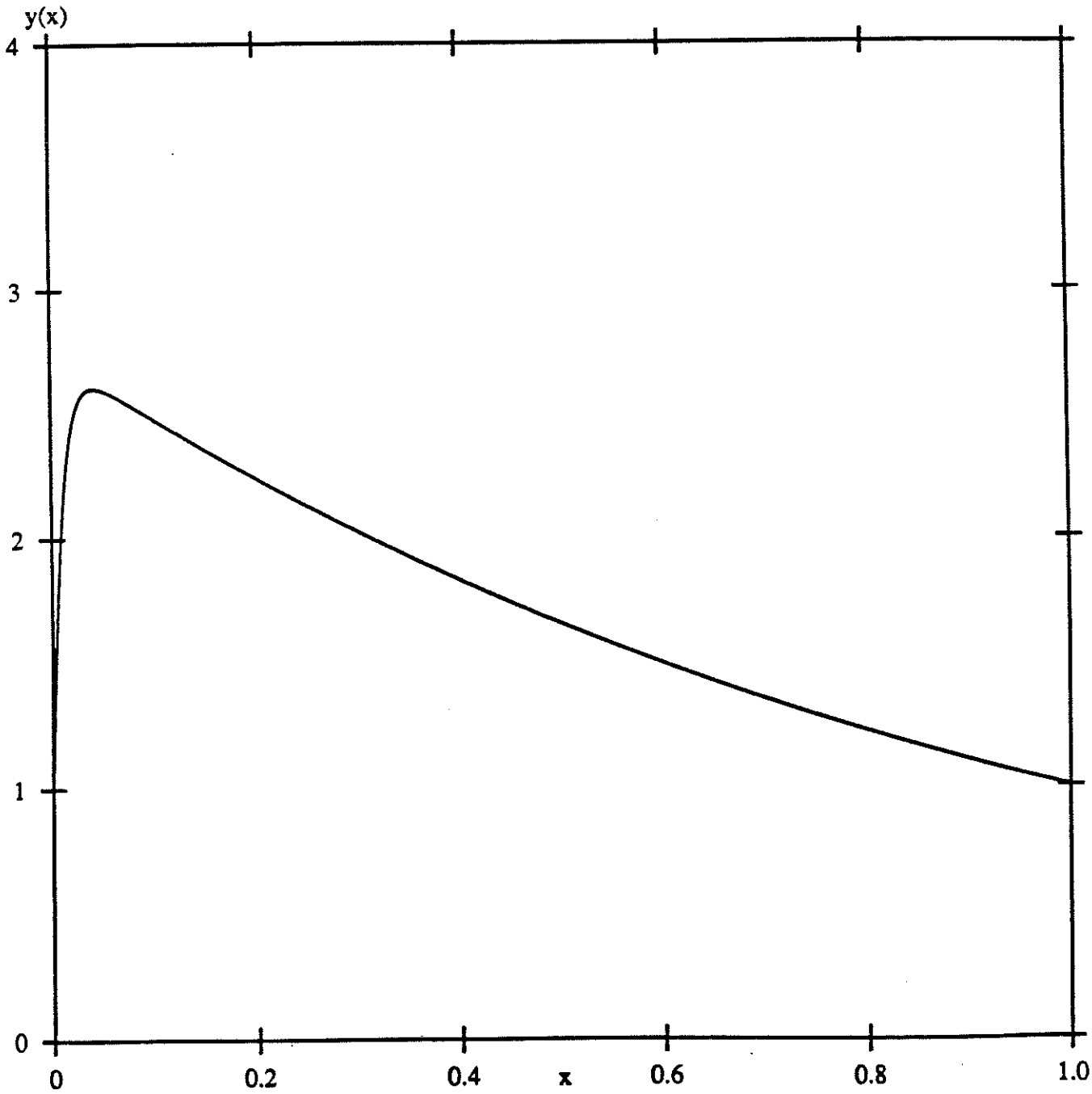

FIGURE 1b

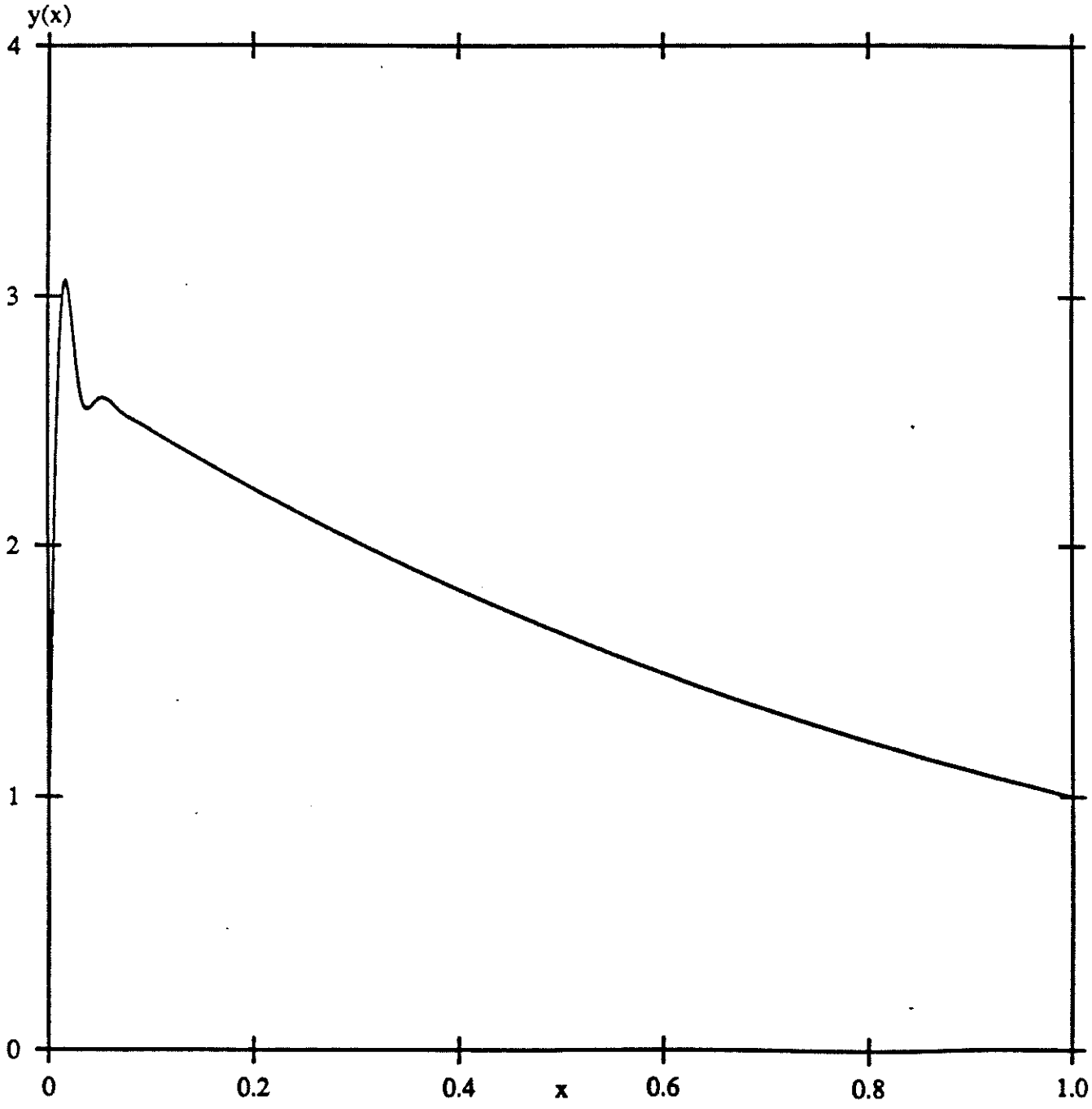

FIGURE 1C

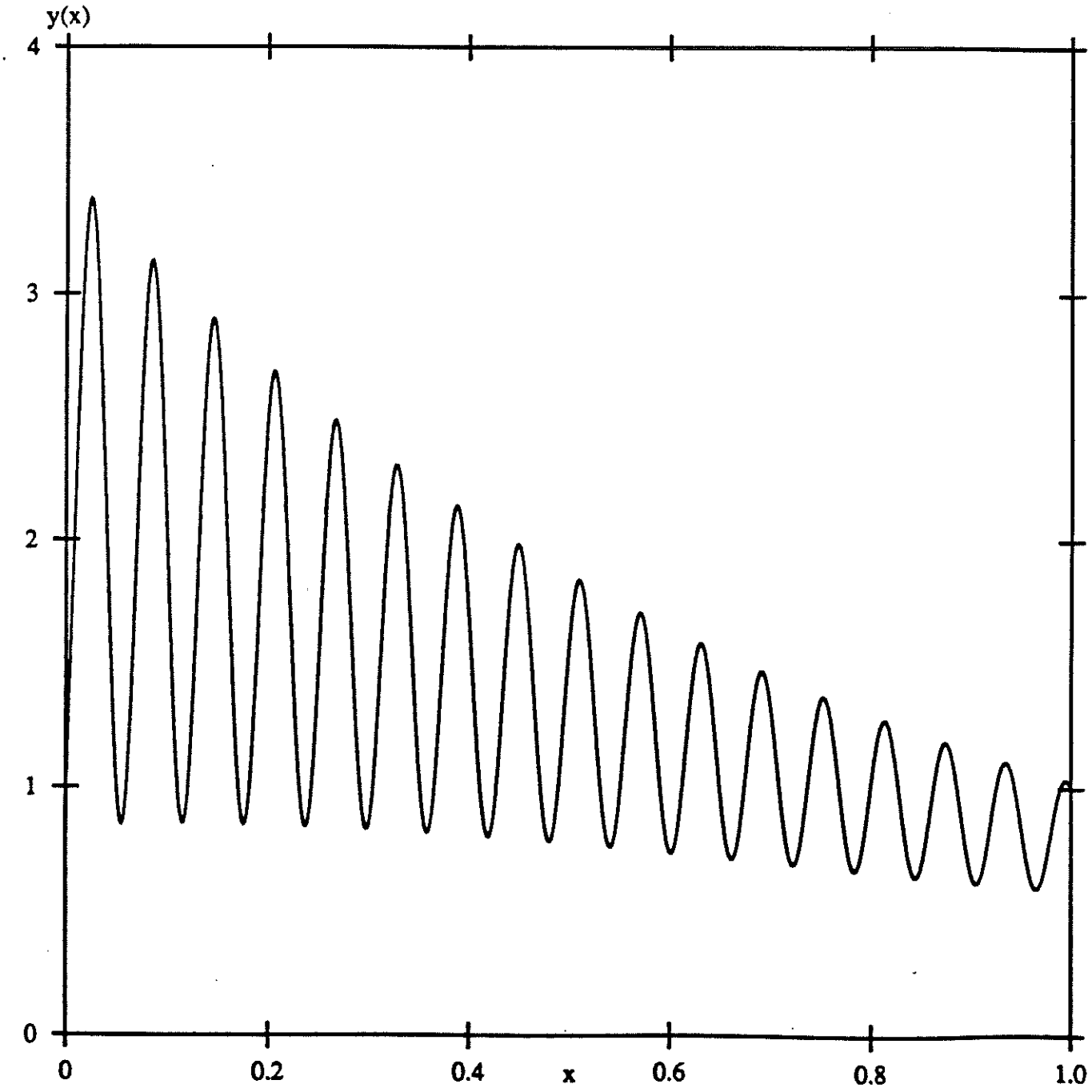

FIGURE 1d

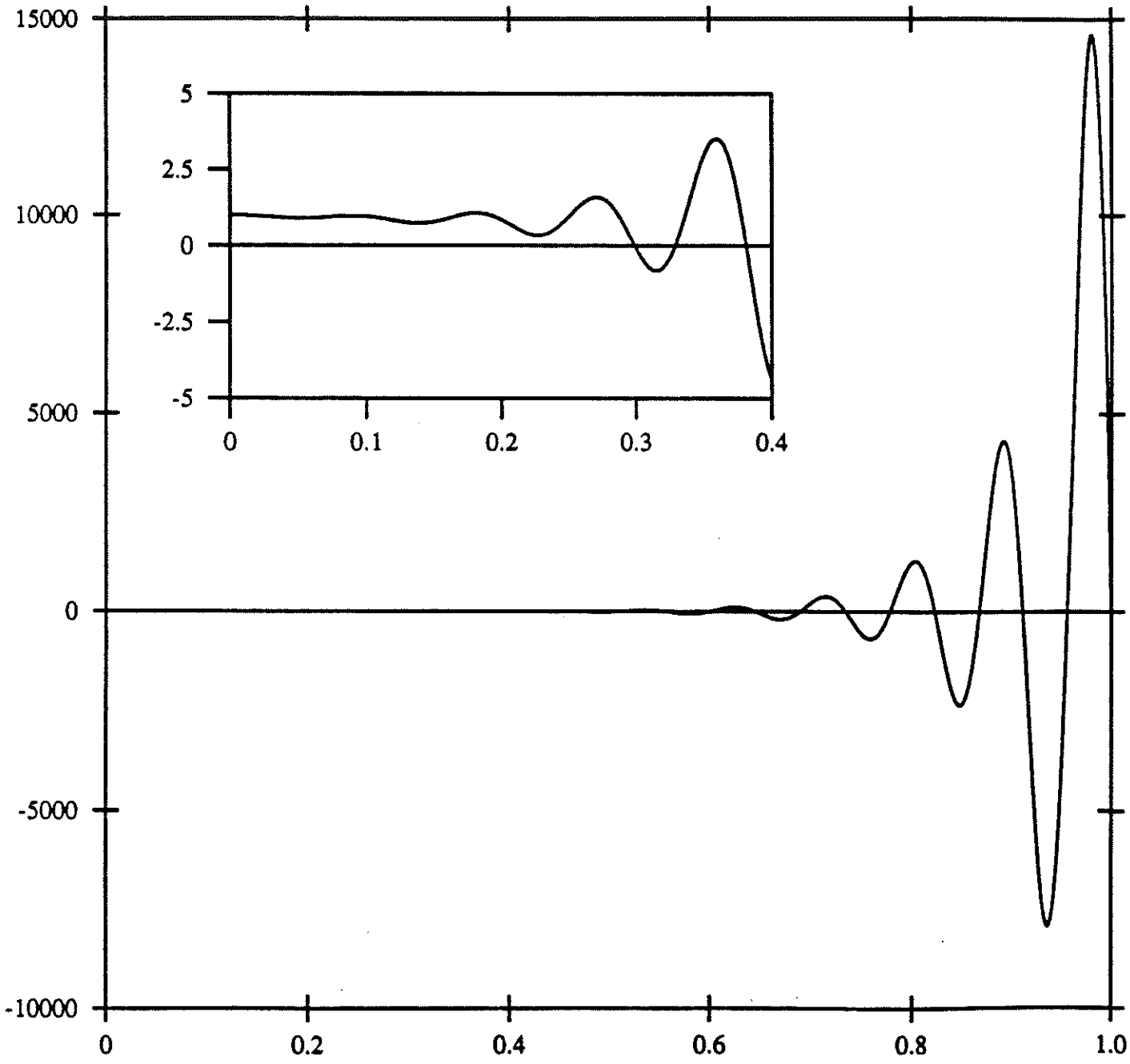
15000
10000
5000
0
-5000
-10000
0
0.2
0.4
0.6
0.8
1.0
5
2.5
0
-2.5
-5
0
0.1
0.2
0.3
0.4

FIGURE 2a

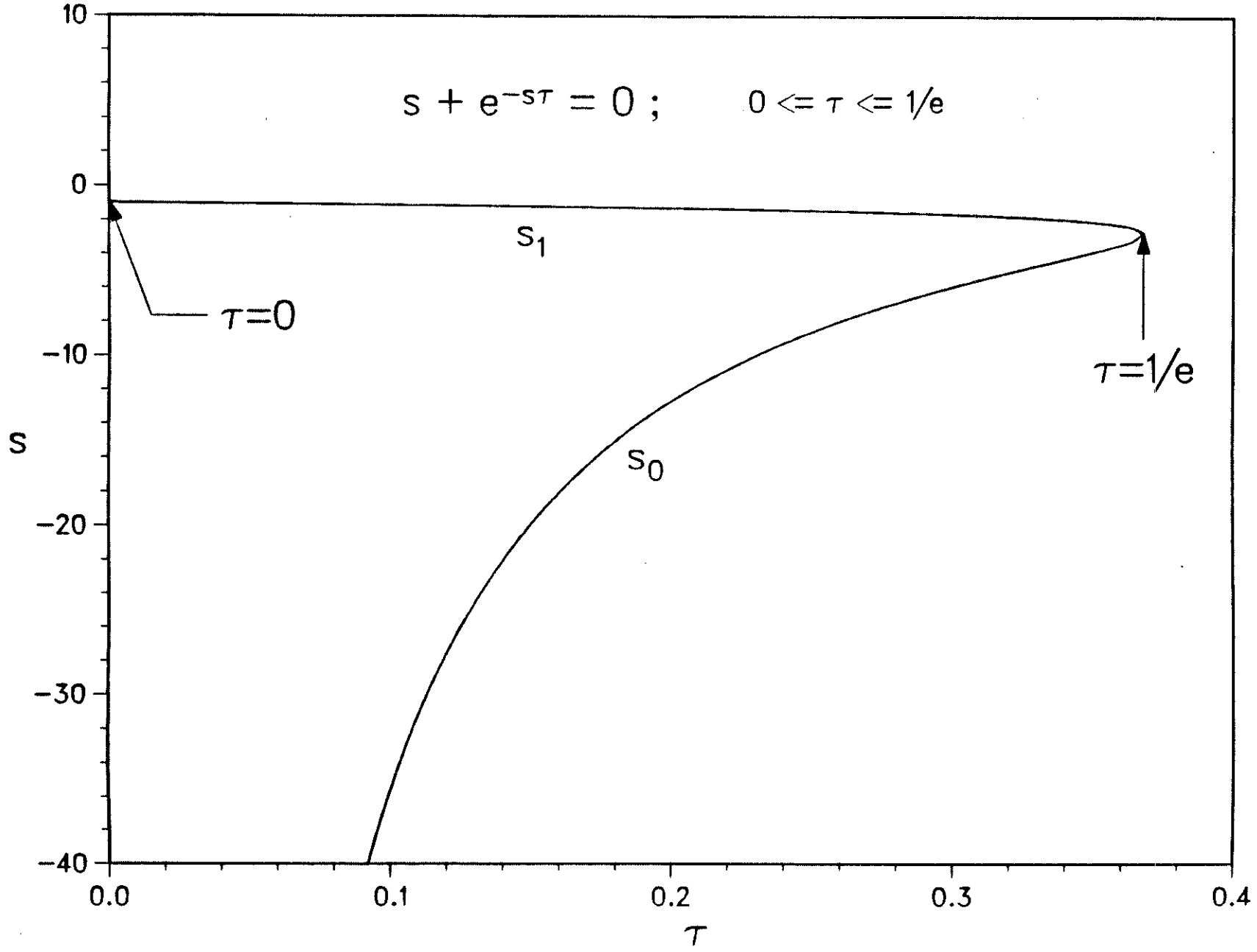
$s + e^{-s\tau} = 0$; $0 <= \tau <= 1/e$
s_1
s_0
$\tau=0$
$\tau=1/e$
s
τ
10
0
-10
-20
-30
-40
0.0
0.1
0.2
0.3
0.4

FIGURE 2b

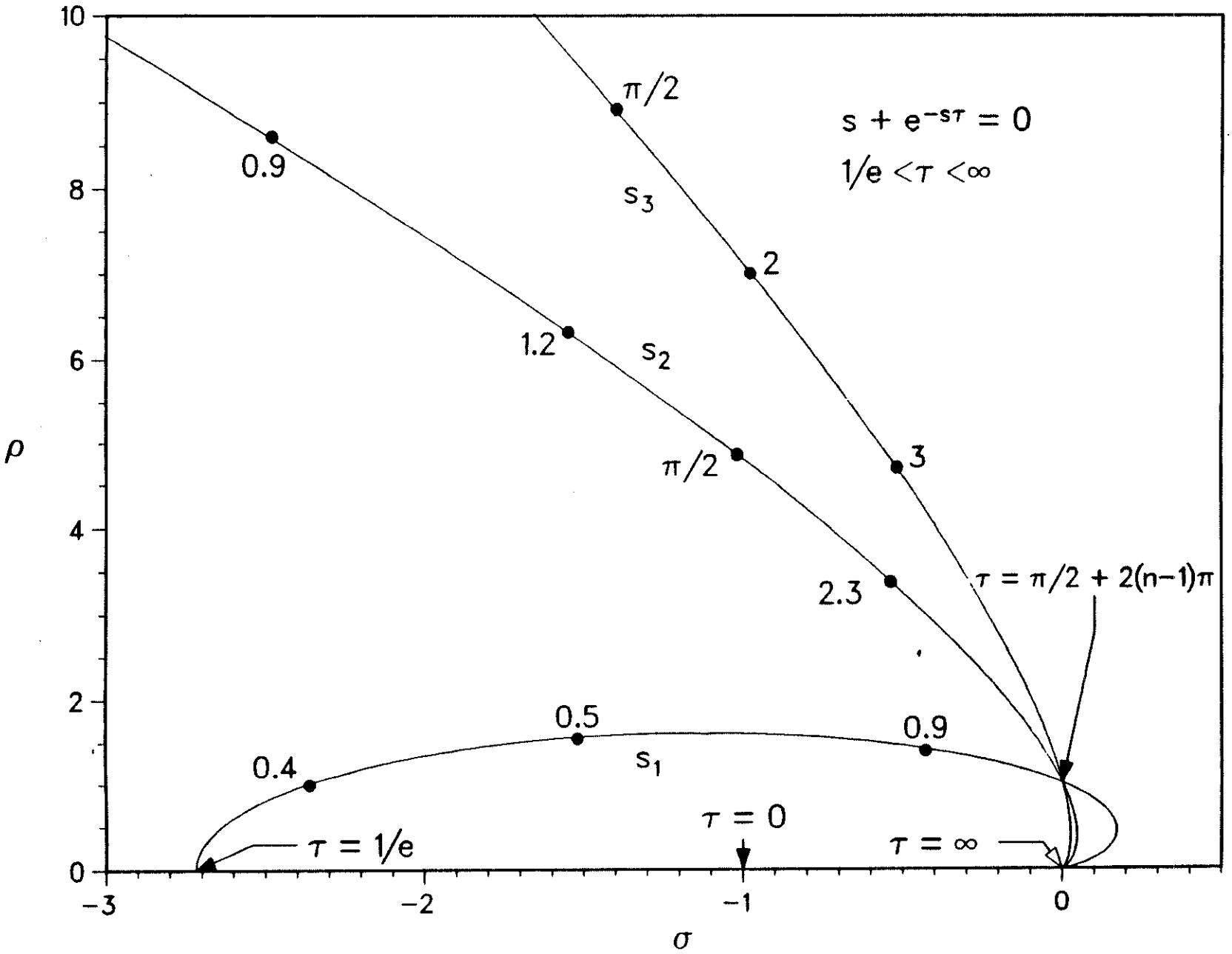
$s + e^{-s\tau} = 0$
$1/e < \tau < \infty$
s_3
s_2
s_1
$\pi/2$
$\pi/2$
0.9
1.2
2
3
2.3
0.5
0.9
0.4
$\tau = 1/e$
$\tau = 0$
$\tau = \infty$
$\tau = \pi/2 + 2(n-1)\pi$
10
8
6
4
2
0
−3
−2
−1
0
ρ
σ

FIGURE 3

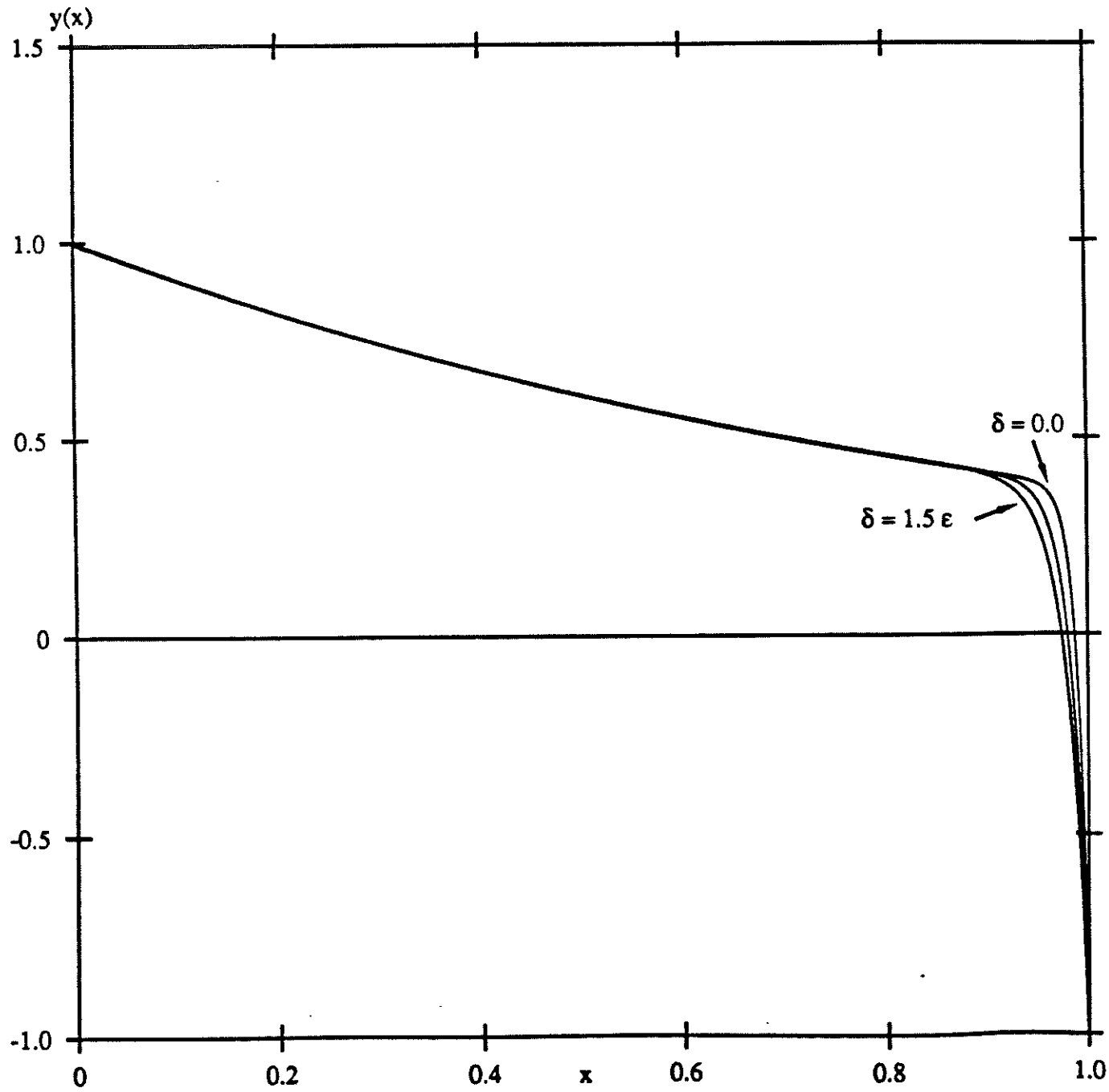

FIGURE 4a

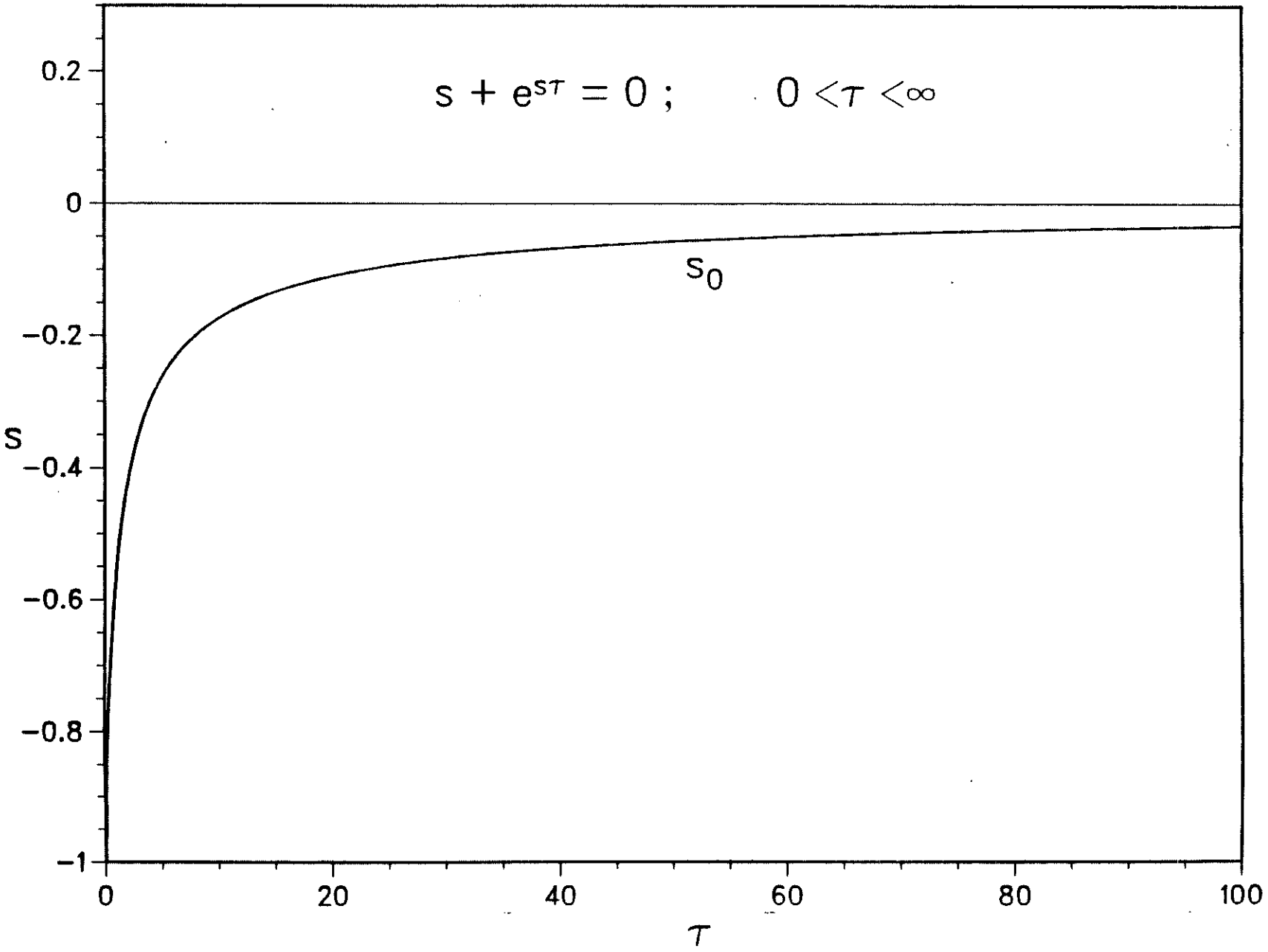
$s + e^{s\tau} = 0\,; \qquad 0 < \tau < \infty$
s_0
0.2
0
−0.2
−0.4
−0.6
−0.8
−1
s
0
20
40
60
80
100
τ

FIGURE 4b

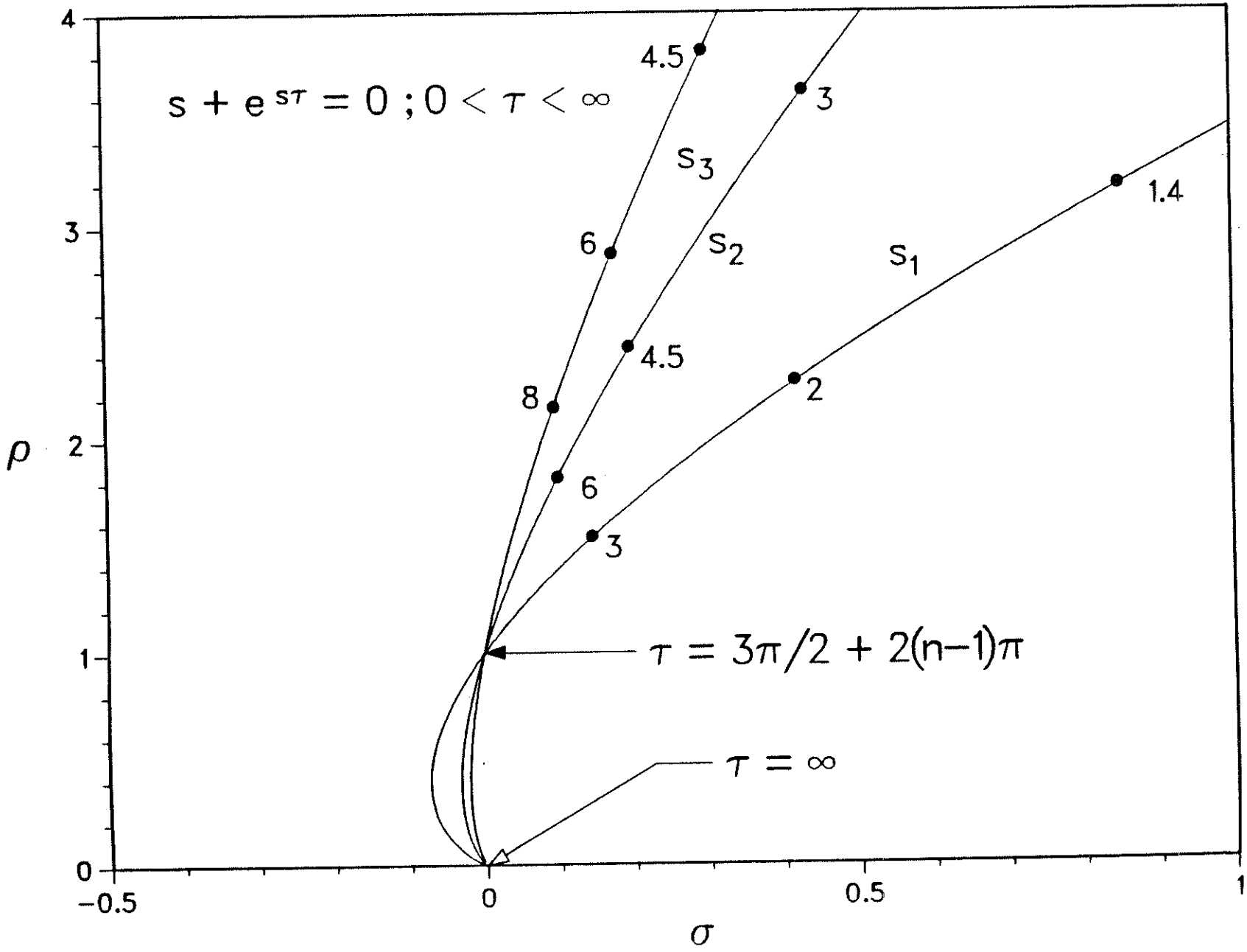
$s + e^{s\tau} = 0 ; 0 < \tau < \infty$
s_3
s_2
s_1
4.5
3
1.4
6
4.5
2
8
6
3
$\tau = 3\pi/2 + 2(n-1)\pi$
$\tau = \infty$
4
3
2
1
0
ρ
−0.5
0
0.5
1
σ

FIGURE 5a

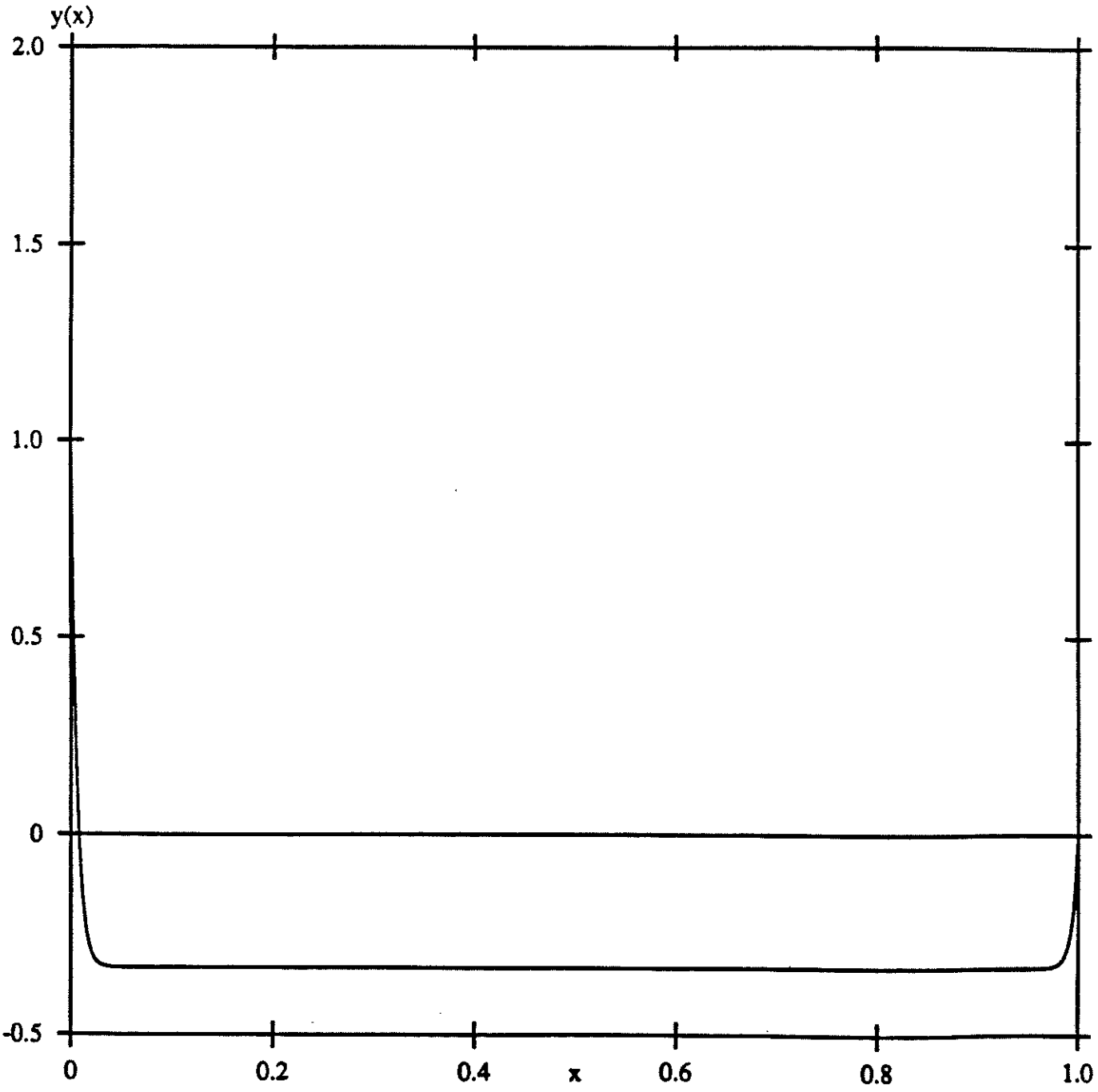

FIGURE 5b

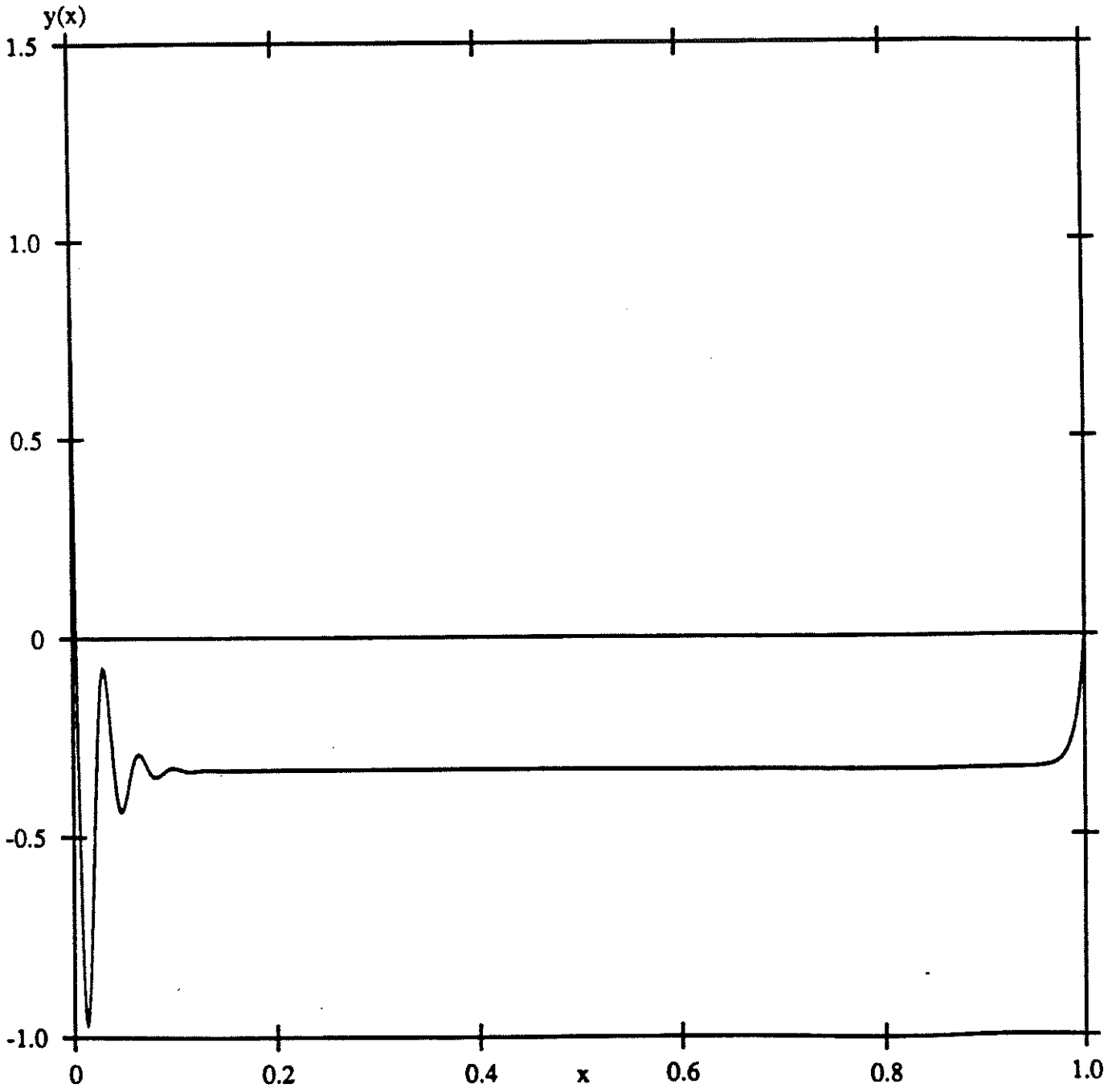

FIGURE 5c

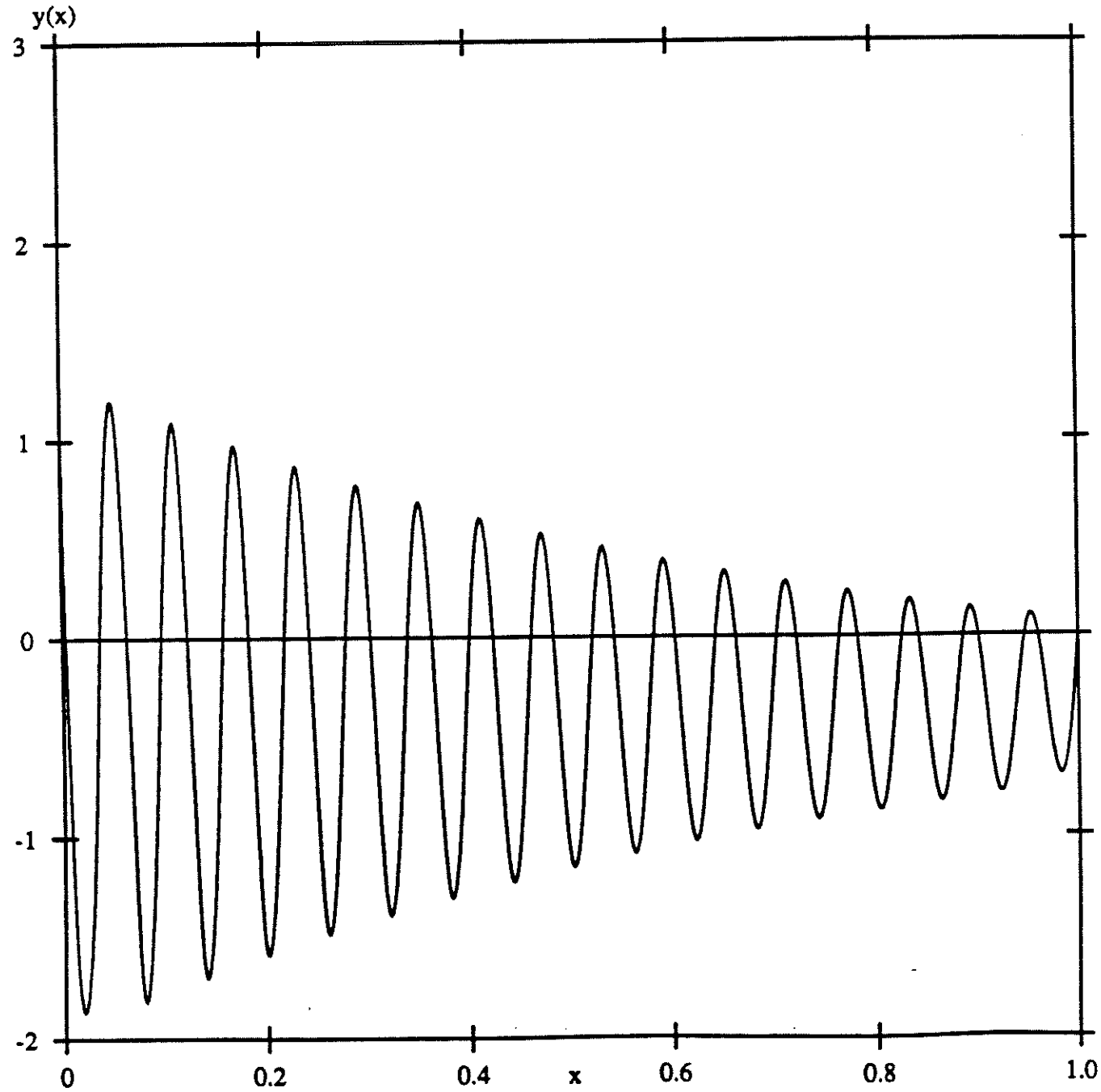

FIGURE 5d

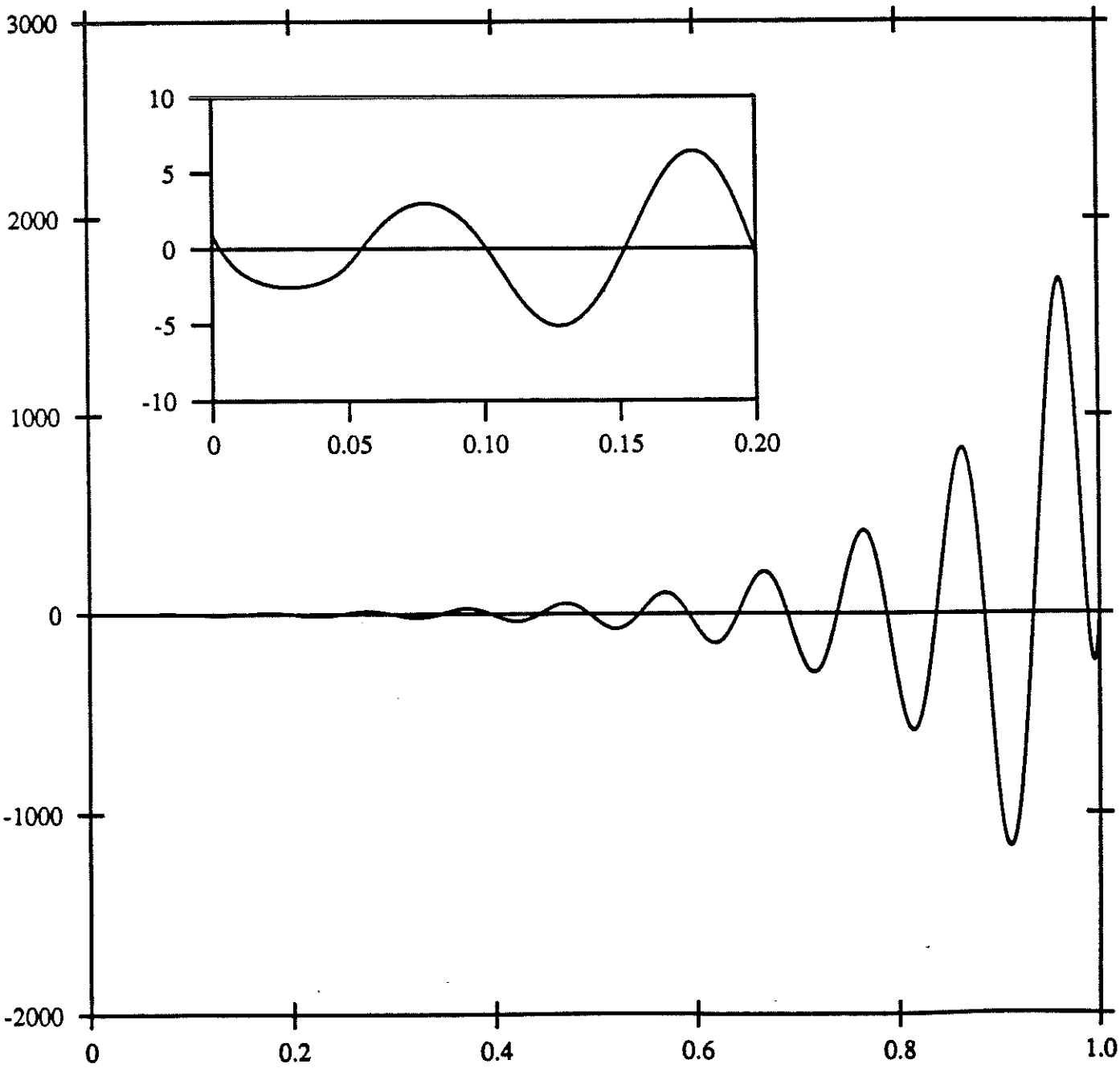
3000
2000
1000
0
-1000
-2000
0
0.2
0.4
0.6
0.8
1.0
10
5
0
-5
-10
0
0.05
0.10
0.15
0.20

FIGURE 6a

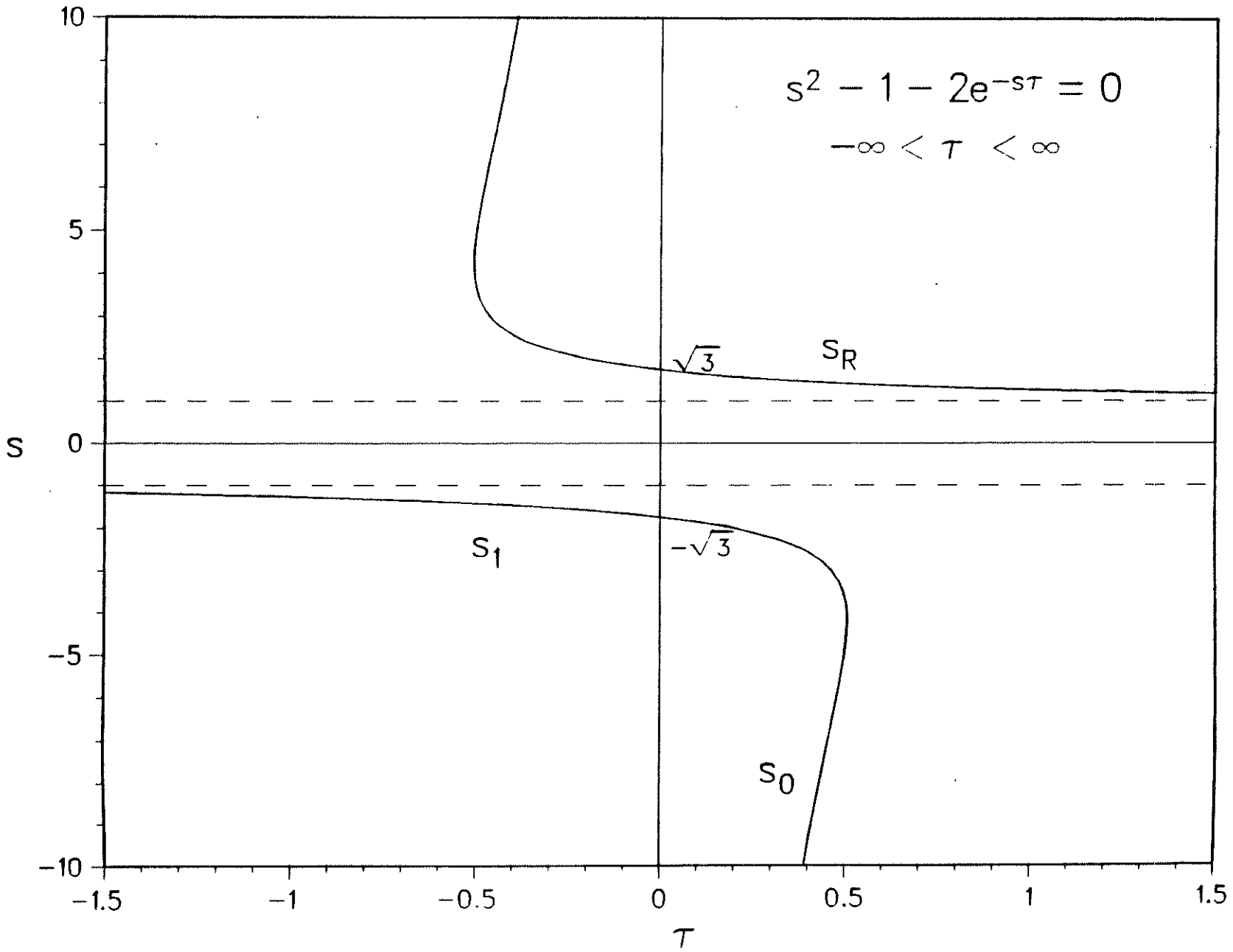
$s^2 - 1 - 2e^{-s\tau} = 0$
$-\infty < \tau < \infty$
s_R
$\sqrt{3}$
s_1
$-\sqrt{3}$
s_0
s
τ
10
5
0
−5
−10
−1.5
−1
−0.5
0
0.5
1
1.5

FIGURE 6b

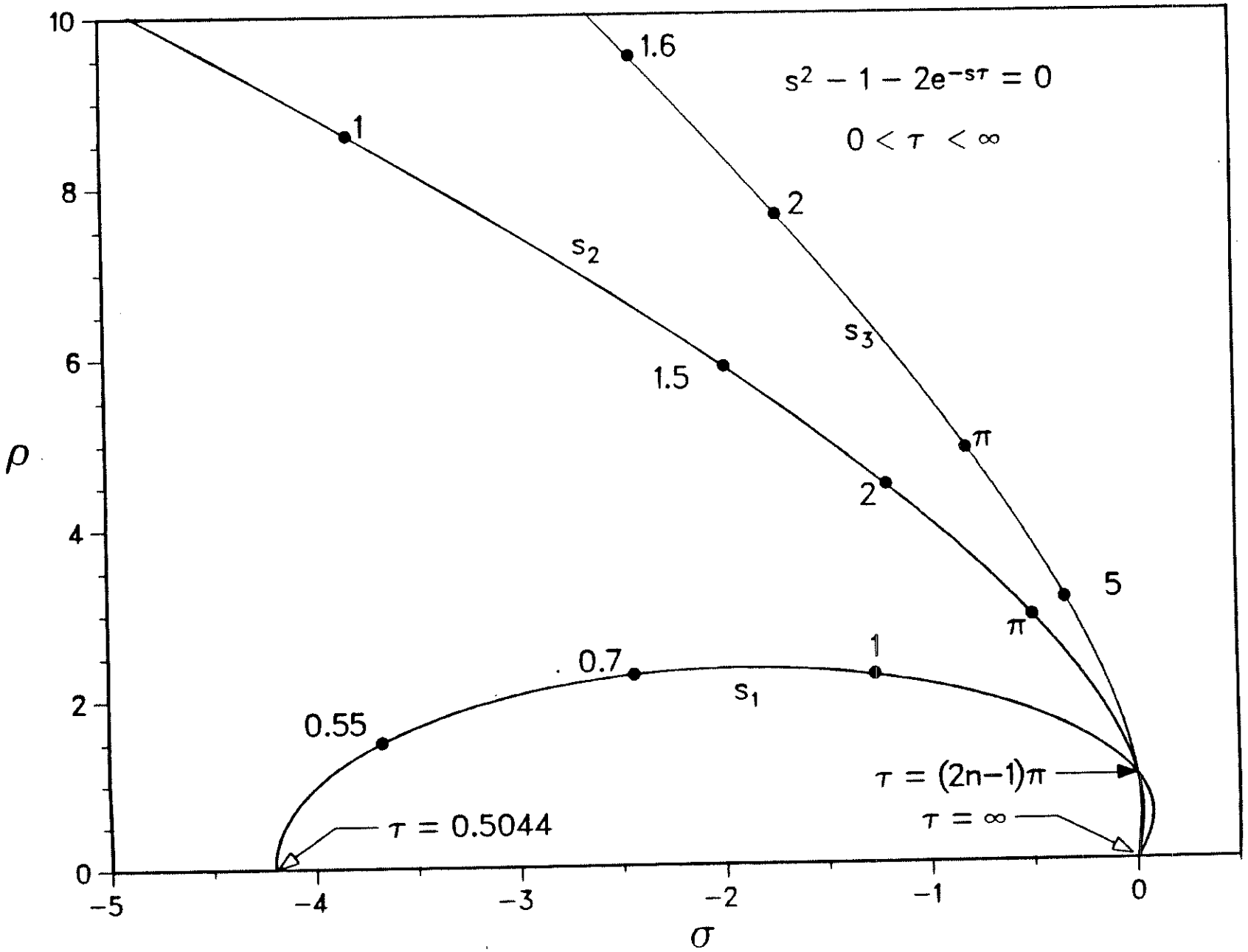
$s^2 - 1 - 2e^{-s\tau} = 0$
$0 < \tau < \infty$
s_1
s_2
s_3
1.6
2
1
1.5
2
π
π
5
1
0.7
0.55
$\tau = 0.5044$
$\tau = (2n-1)\pi$
$\tau = \infty$
ρ
σ
10
8
6
4
2
0
−5
−4
−3
−2
−1
0

FIGURE 6C

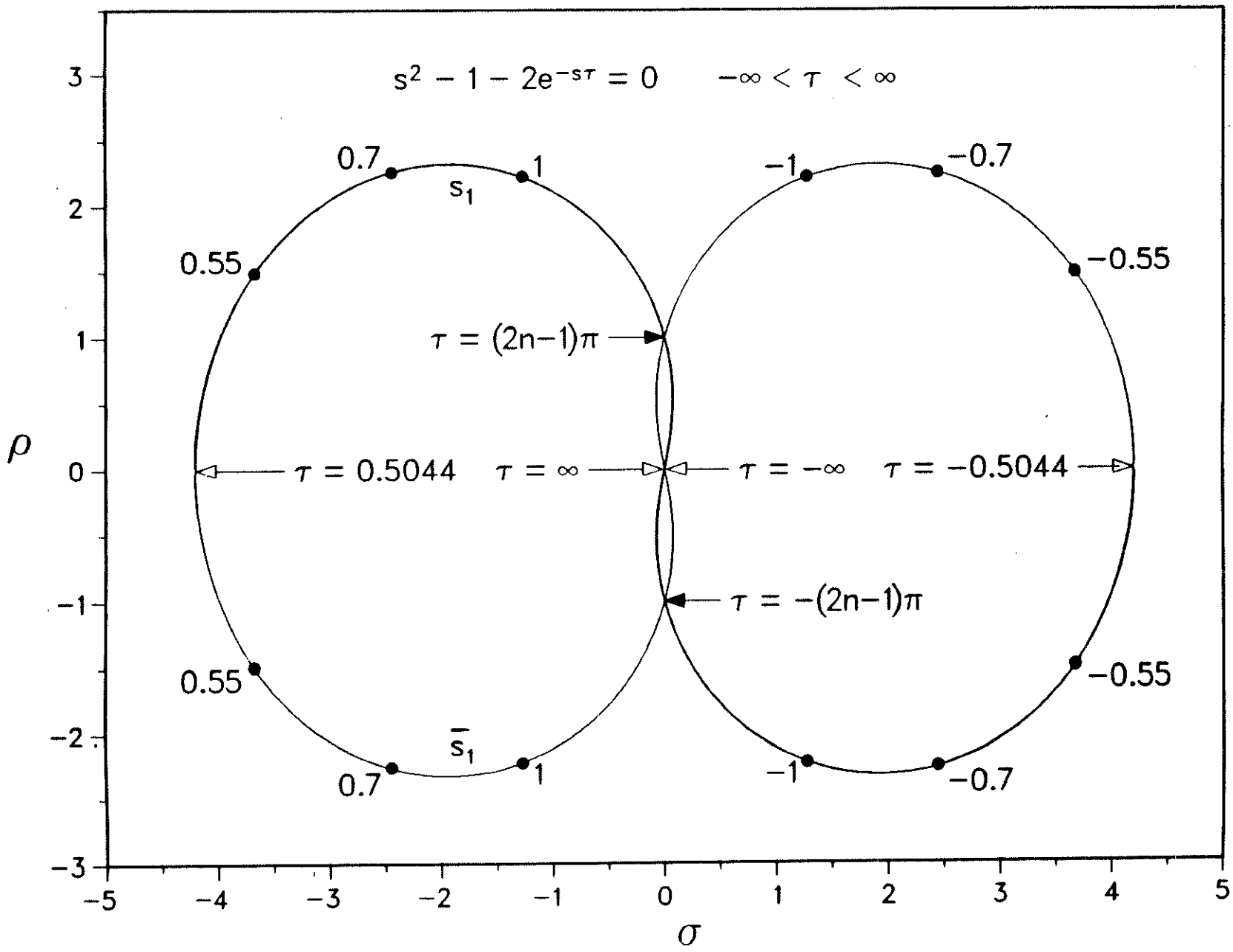
$s^2 - 1 - 2e^{-s\tau} = 0 \quad -\infty < \tau < \infty$
0.7
1
s_1
0.55
$\tau = (2n-1)\pi$
$\tau = 0.5044$
$\tau = \infty$
$\tau = -\infty$
$\tau = -0.5044$
$\tau = -(2n-1)\pi$
$\bar{s}_1$
−1
−0.7
−0.55
ρ
σ

FIGURE 7a

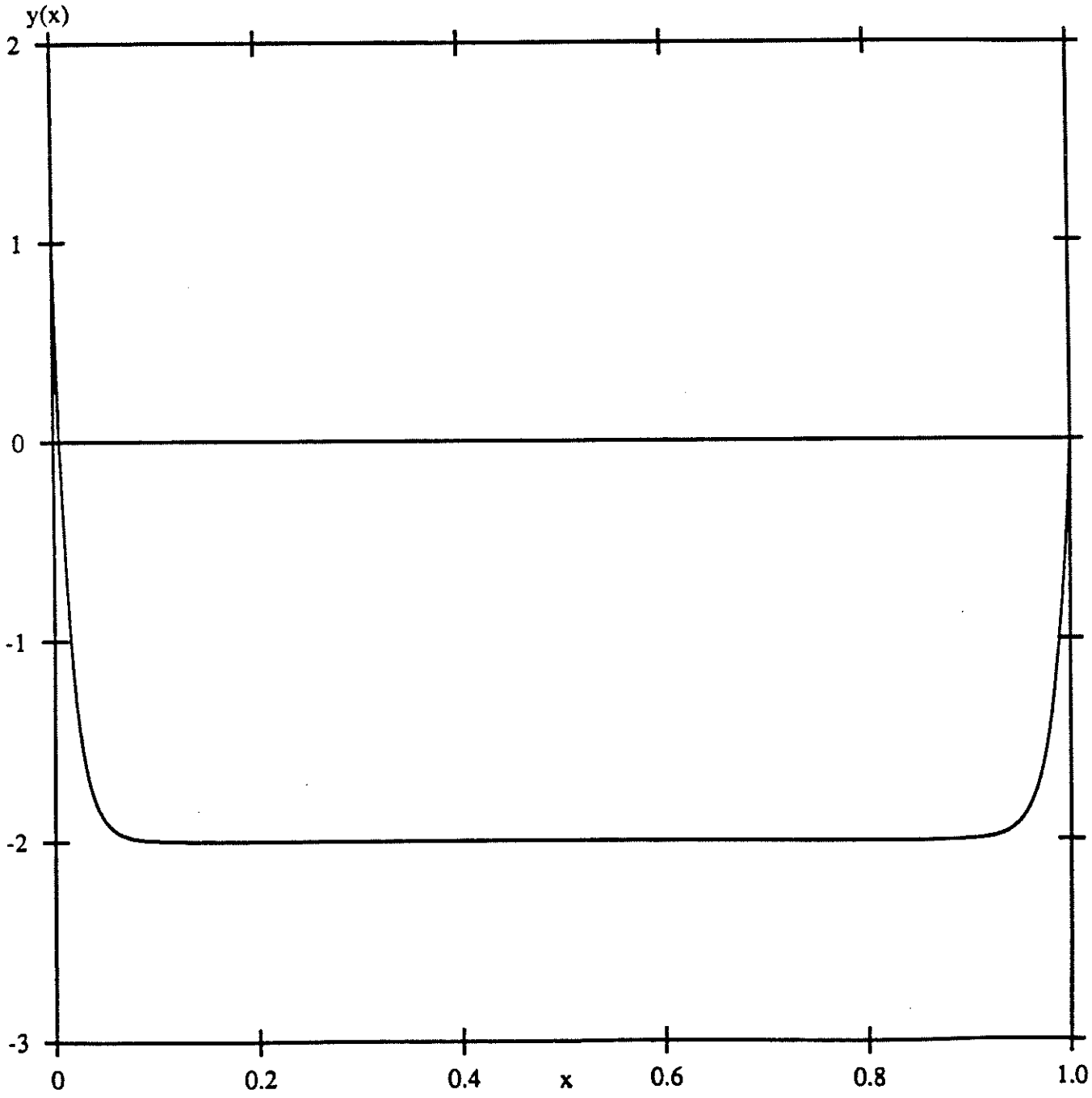

FIGURE 7b

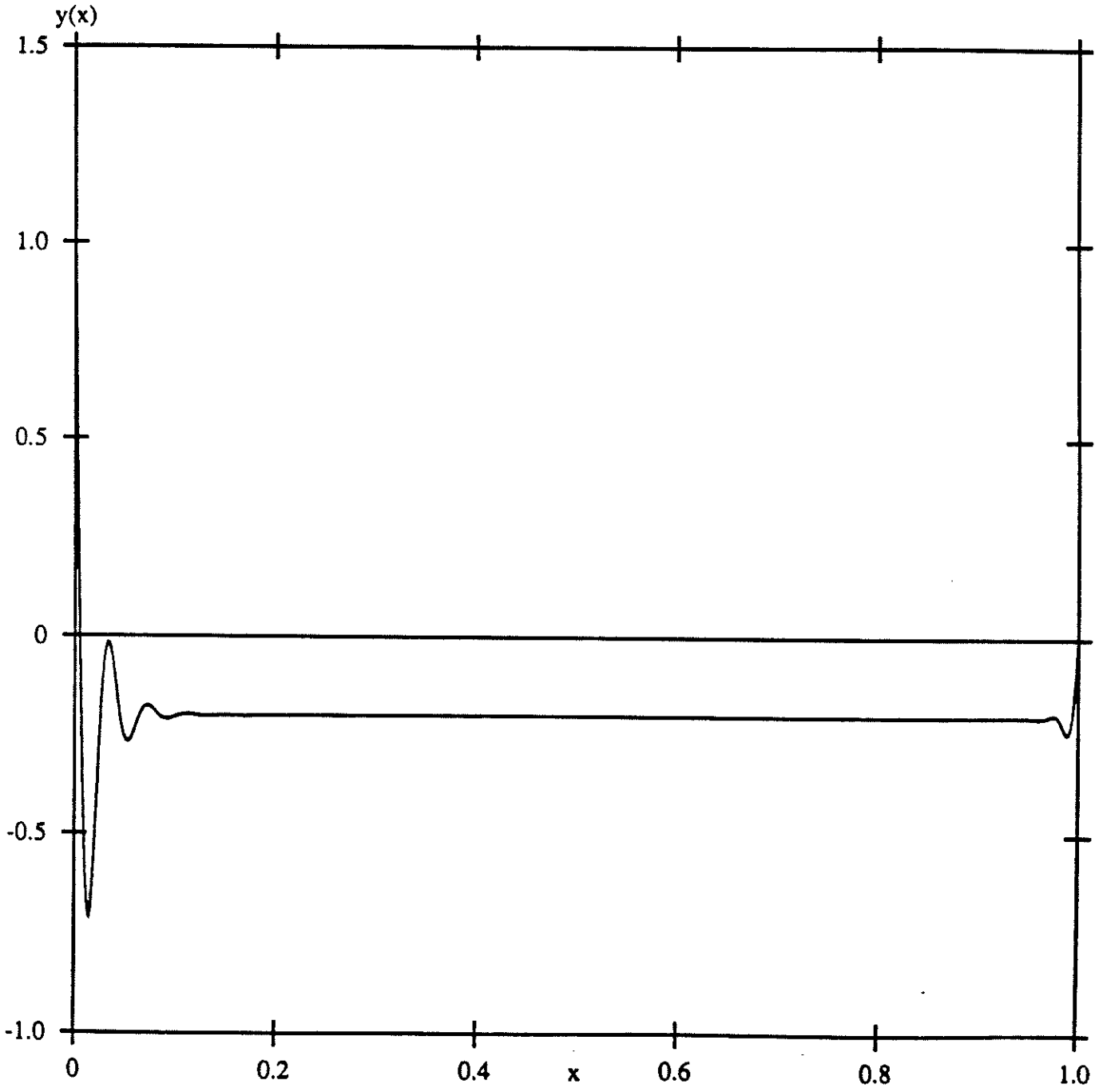

FIGURE 8a

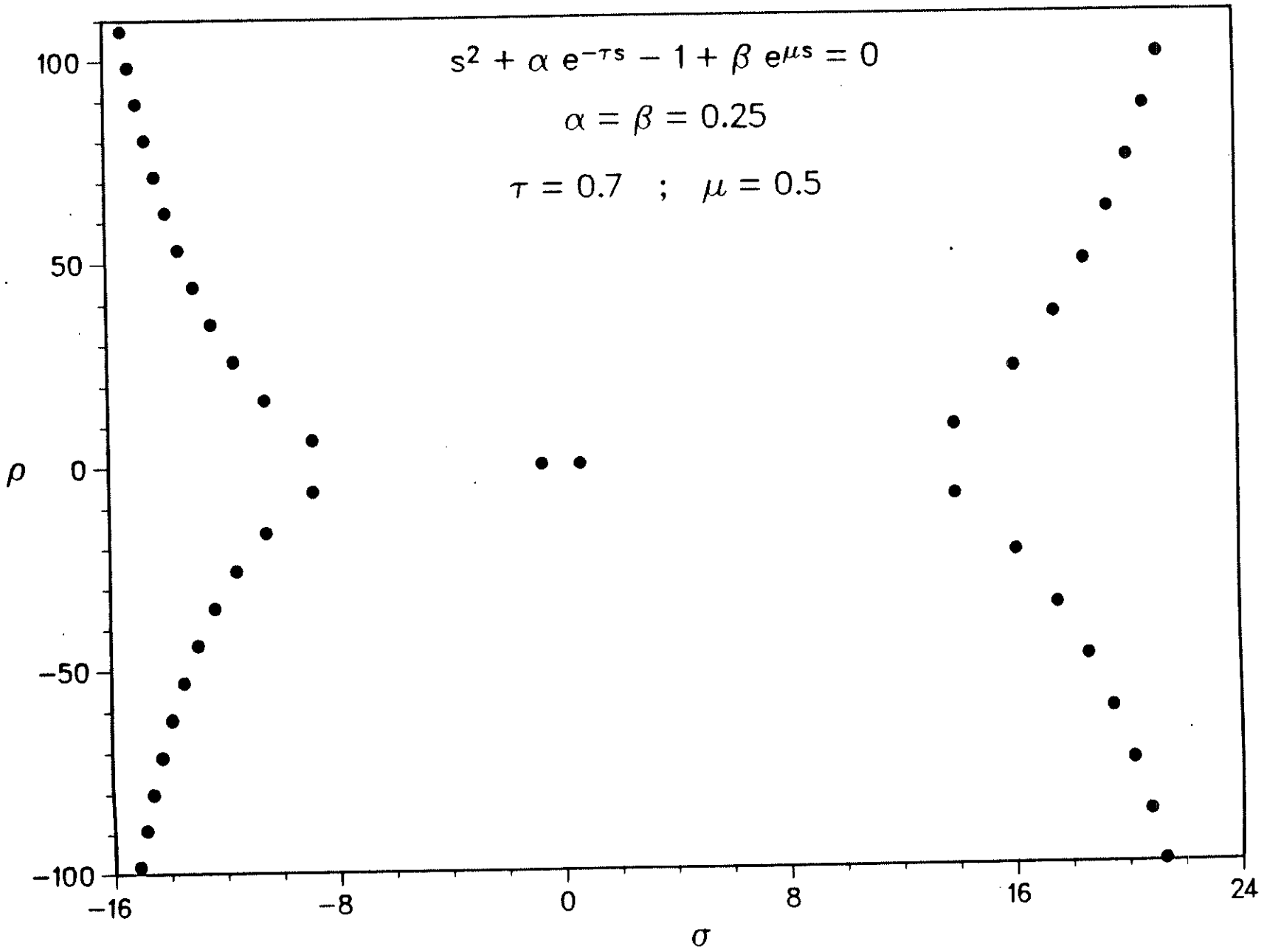
$s^2 + \alpha\, e^{-\tau s} - 1 + \beta\, e^{\mu s} = 0$
$\alpha = \beta = 0.25$
$\tau = 0.7 \quad ; \quad \mu = 0.5$
100
50
0
−50
−100
ρ
−16
−8
0
8
16
24
σ

FIGURE 8b

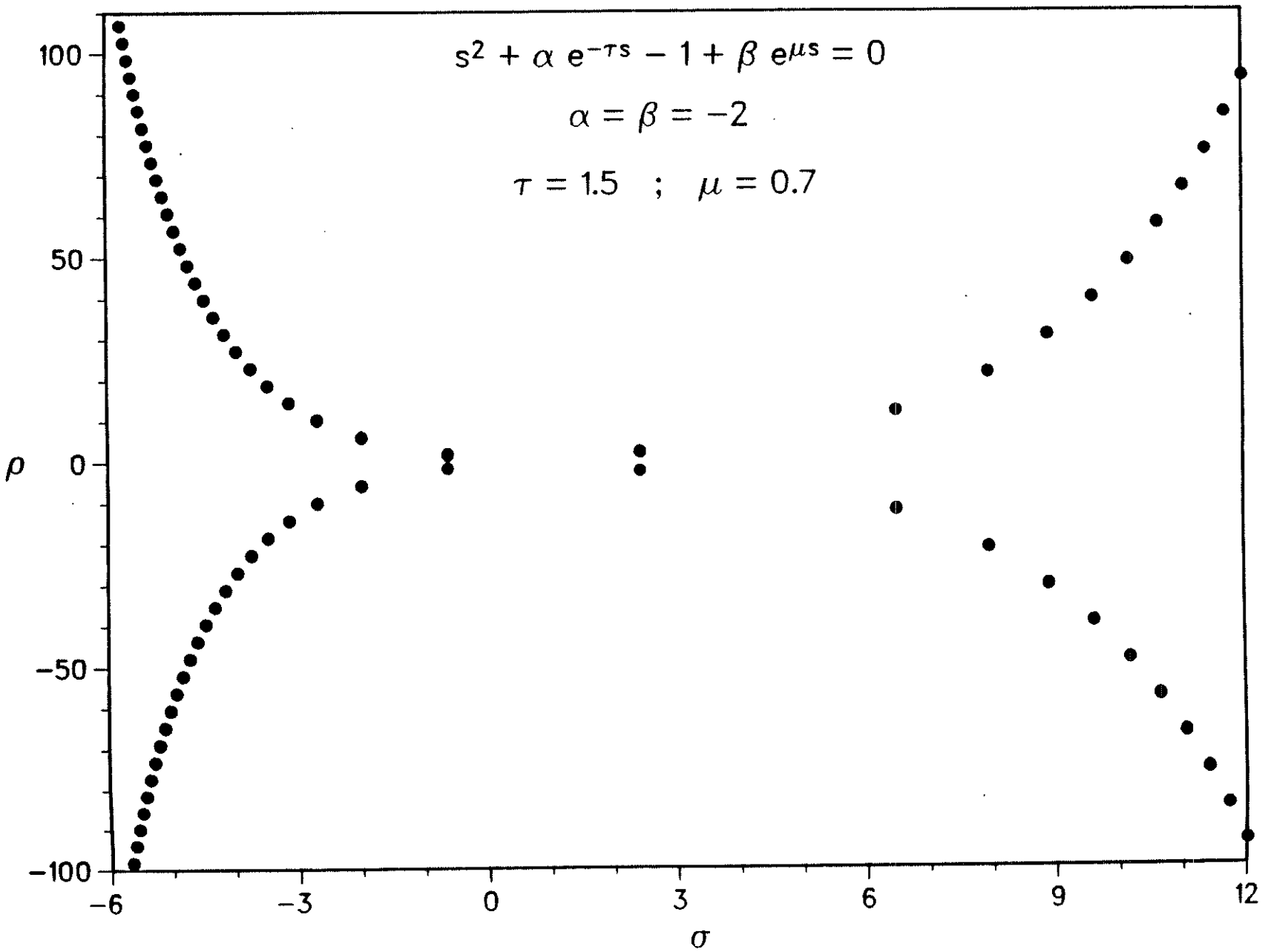
$s^2 + \alpha\, e^{-\tau s} - 1 + \beta\, e^{\mu s} = 0$
$\alpha = \beta = -2$
$\tau = 1.5 \quad ; \quad \mu = 0.7$
100
50
0
−50
−100
ρ
−6
−3
0
3
6
9
12
σ